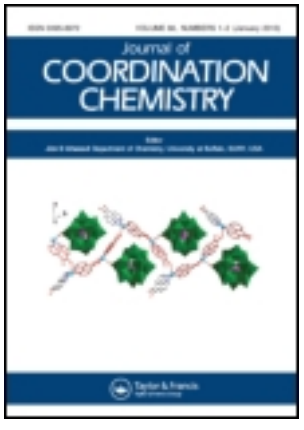

Journal of Coordination Chemistry
Publication details, including instructions for authors and subscription information:
http://www.tandfonline.com/loi/gcoo20

Coordination and organometallic compounds as precursors of classic and less-common nanostructures: recent advances

Boris I. Kharisov[ac], Oxana V. Kharissova[b] & Ubaldo Ortiz Méndez[c]

[a] Facultad de Ciencias Químicas, Universidad Autónoma de Nuevo León, Monterrey, México

[b] Facultad de Ciencias Físico-Matemáticas, Universidad Autónoma de Nuevo León, Monterrey, México

[c] CIIDIT, Universidad Autónoma de Nuevo León, Monterrey, México

Accepted author version posted online: 08 Oct 2013.Published online: 15 Nov 2013.

To cite this article: Boris I. Kharisov, Oxana V. Kharissova & Ubaldo Ortiz Méndez (2013) Coordination and organometallic compounds as precursors of classic and less-common nanostructures: recent advances, Journal of Coordination Chemistry, 66:21, 3791-3828, DOI: 10.1080/00958972.2013.851382

To link to this article: http://dx.doi.org/10.1080/00958972.2013.851382

Journal of Coordination Chemistry, 2013
Vol. 66, No. 21, 3791–3828, http://dx.doi.org/10.1080/00958972.2013.851382

Coordination and organometallic compounds as precursors of classic and less-common nanostructures: recent advances

BORIS I. KHARISOV†§, OXANA V. KHARISSOVA*‡ and UBALDO ORTIZ MÉNDEZ§

†Facultad de Ciencias Químicas, Universidad Autónoma de Nuevo León, Monterrey, México
‡Facultad de Ciencias Físico-Matemáticas, Universidad Autónoma de Nuevo León, Monterrey, México
§CIIDIT, Universidad Autónoma de Nuevo León, Monterrey, México

(*Received 18 May 2013; accepted 18 September 2013*)

The synthesis of various classic and less-common inorganic nanostructures (nanoparticles, microflowers, nanourchins, nanofilms, nanorods, nanoleaves, nanowires, etc.) consisting mainly of elemental metals, intermetallics, oxides and sulfides from metal complexes as precursors is reviewed. To prepare nanoparticles/nanostructures, a series of complexes of N–, O–, S–, N, O–, N, S(Se)–, and N, P-containing ligands, as well as σ- and π-organometallic compounds of mainly transition metals have been treated using pyrolysis, laser, ultrasonic irradiation, CVD techniques, electron beam irradiation, and related sophisticated techniques from 100 to 700 °C. The obtained nanoparticles possess a series of useful applications, in particular as catalysts, sensors, sorbents, and remediation agents.

Keywords: Nanostructures; Coordination compounds; Organometallics; Pyrolysis; Decomposition

Introduction

Metal complexes have useful applications in organic and organometallic chemistry, catalysis, medicine as anticancer pharmaceutics and for drug delivery, in various biological systems, polymers and dyes, separation of isotopes and heavy metals, among many others. Coordination and organometallic compounds serve as precursors for a series of elemental metals in pyrophoric form, as their oxides, salts, and doped inorganic compounds by thermal decomposition and other methods. Frequently, depending on reaction conditions, the products are formed in nanostructured shapes (spherical particles, nanorods, nanowires, nanofibers, nanosheets, nanosponge, and more unusual nanostructures). In particular, porous metal–organic frameworks may be suitable precursors for the simple one-pot preparation of nanoscale metal oxide materials with different and interesting morphologies. Particular aspects of this field were covered in excellent recent reviews [1, 2]. In the present generalization, we have tried to present the most recent advances on application of metal complexes for fabrication of distinct nanostructures having already explored or potential applications. We note in advance that in a difference with classic metal complexes/coordination compounds where a simple pyrolysis technique or other low-temperature or high-temperature methods have been applied

*Corresponding author. Email: bkhariss@mail.ru

for nanoparticle processing, metal–organic chemical vapor deposition (MOCVD), plasma CVD, electron beam irradiation, combustion, laser, and related sophisticated techniques are mainly utilized for organometallics {the ligands are usually cyclopentadienyl (Cp), alkyl, carbonyl, 1,3-cyclooctadiene (COD), and 1,3,5-cyclooctatriene (COT) among others}. The material systematization has been carried out according to the chemical composition of resulting nanostructures, paying particular attention to the ligand type (N–, O–, N, O–, N, S–, N, P-containing moieties), bond type (coordination bond M–O, M–N, M–S(Se), M–P, σ- and π- metal-carbon bond), and applied synthesis/decompositon method (pyrolysis, microwave heating, CVD, laser, ultrasonic and plasma techniques, low-temperature methods, etc.).

Metals and metal composites

Elemental nanosized metals are represented by a relatively large number of reports, although less in comparison with the heart of nanotechnology – metal oxides. Starting from coordination compounds and organometallics, they (1) have been fabricated in free and supported forms, (2) are mainly transition metals, and (3) are mainly noble metals (although several non-noble transition metals as iron, cobalt, or copper have also been synthesized from metal complexes), and (4) can be bimetallic nanoparticles. High numbers of noble nanostructured metals can be explained by thermodynamic instability of their oxides in the conditions of pyrolysis (main method for destruction of metal complex precursors). On the contrary, in case of other transition metals, their most stable phases are generally oxides.

The most frequently reported noble nanometals are palladium and platinum (in particular, in bimetallic form), obtained from complexes with N–, O–, and P-containing ligands and organometallics; this is not surprising due to numerous applications of these two metals, in particular in catalysis. Thus, the highly porous metal organic framework MOF-5 was loaded with $[Pd(C_3H_5)(C_5H_5)]$ by MOCVD resulting in the inclusion compound $[Pd(C_3H_5)(C_5H_5)]$@MOF-5 [3]. Ultrasmall Pd nanoparticles of 2–5 nm in size were formed inside the cavities of MOF-5 by its hydrogenolysis at r.t. In the Suzuki coupling reaction, the Pd@MOF-5 materials showed good activity in the first catalytic run, destroying the crystal structure of MOF-5 during the following reaction runs, which caused loss of activity. Another example of a supported palladium(0) nanomaterial is a carbon nanosheet (CNS)-Pd nanosized particle composite, synthesized [4] by using graphite oxide (GO) and *bis*(ethylenediamine) palladium(II) $\{Pd(en)_2^{2+}\}$ (figure 1) as precursors. It was found that the $Pd(en)_2^{2+}$ complex ions can be intercalated into GO layers highly efficiently to form a layered structure containing a large amount of Pd (~12 wt.%). By subsequent chemical reduction, Pd nanoparticles (2–6 nm in size) are well dispersed between CNS to form a CNS-Pd nanoparticle composite and serve as spacers to increase the porosity of the composite. This unique composite nanostructure having large contents of Pd nanoparticles (20–25 wt.%) stabilized by CNSs may be applied to the fields of H_2-related catalysis and sensing.

Two compounds based on $O_3PCH_2PO_3^{4-}$ ligands and $\{Mo^V_2O_4\}$ dimeric units, $(NH_4)_{18}[(Mo_2O_4)_6(OH)_6(O_3PCH_2PO_3)_6]\cdot 33H_2O$ and $Na_8[(Mo_2O_4)_3(O_3PCH_2PO_3)_3(CH_3AsO_3)]\cdot 19H_2O$, were very efficient both as reductants of Pt and Pd metallic salts and as capping agents for the resulting Pt^0 and Pd^0 nanoparticles [5]. The size of the obtained nanoparticles depends both on the nature of the polyoxometalate and on the [metallic salt]/[POM] ratio. The presence of Mo^{VI} species was revealed in both cases that stabilize the nanoparticles and the absence of Mo^V moieties; the capping Mo^{VI} polyoxometalates are identical for both systems and contain the diphosphonato ligand.

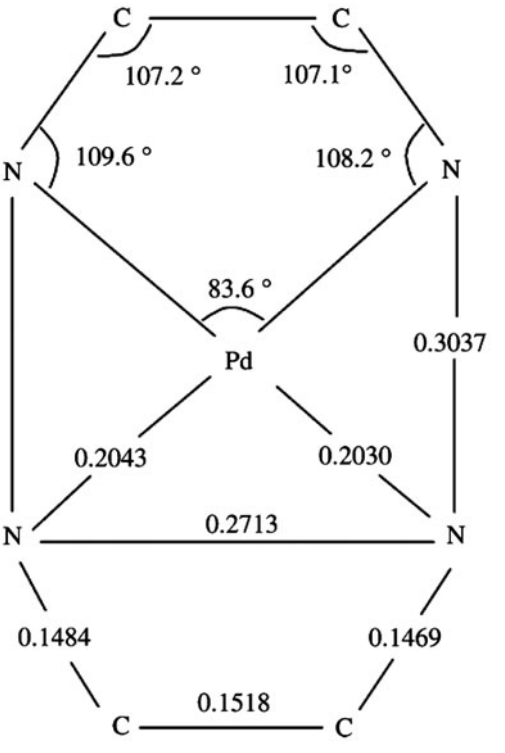

Figure 1. Structure of the planar $Pd(en)_2^{2+}$ complex (units of bond length: nm).

Also, *tris*(dibenzylideneacetone)dipalladium {$Pd_2(dba)_3$, dba = dibenzylideneacetone **1**} was used as a source of soluble Pd species for catalysis and as a precursor in the synthesis of more complex Pd structures [6, 7]. Synthesis of platinum nanoparticles (2–3 nm) generated from the related complex $Pt_2(dba)_3$ {*tris*(dibenzylideneacetone)diplatinum}, stabilized with a long alkyl chain amine, hexadecylamine (HDA), and supported on functionalized single-walled carbon nanotubes (SWCNTs) was described [8]. The presence of the stabilizer at the surface of the Pt nanoparticles was confirmed even after the purification step and functional groups at the surface of pre-treated SWCNTs. A solid solution of platinum(II) and palladium(II) oxalato-complex, $(NH_4)_2[Pt_{0.5}Pd_{0.5}(C_2O_4)_2]\cdot 2H_2O$, was synthesized [9] and studied as a precursor for preparing small homogeneous bimetallic PtPd nanoparticles through its thermal decomposition in hydrogen and helium atmospheres. The annealing temperature and time had little effect on the bimetallic particle size.

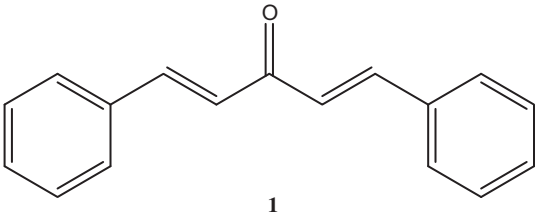

1

The effect of 500 eV electrons on nanometer-scale-thick films of trimethyl(methylcyclopentadienyl)platinum(IV) ($MeCpPt^{IV}Me_3$) were studied *in situ* under ultra-high vacuum conditions [10]. The electron beam induced decomposition of adsorbed $MeCpPt^{IV}Me_3$ produced a carbonaceous film that contained Pt in an electronic state intermediate between metallic Pt and Pt(IV). In addition to Pt(IV) reduction, electron beam irradiation was also accompanied by evolution of methane and hydrogen from the adsorbate layer and the loss of C–H groups (figure 2). A comparison of the gas-phase products observed during electron irradiation of adsorbed $MeCpPt^{IV}Me_3$ and $CpPt^{IV}Me_3$ supported the idea that electron-stimulated decomposition of these platinum precursors occurs by Pt-CH_3 bond cleavage. Despite the ejection of methane, it should be emphasized that the majority of the carbons initially associated with $MeCpPt^{IV}Me_3$ become incorporated into the Pt-containing amorphous carbon film that forms as a result of electron irradiation. The average reaction cross section for adsorbed $MeCpPt^{IV}Me_3$ exposed to 500 eV electrons was calculated to be 2.2×10^{-16} cm^2. The overall surface reaction 1 can be expressed as follows.

$$MeCpPt^{IV}Me_{2(ads\cdot)} + e^- \rightarrow PtC_{8(ads\cdot)} + H_{2(g)} \uparrow + CH_4 \uparrow \quad (1)$$

Other noble metals are more rarely produced from metal complexes, generally from π-organometallics. Thus, Ru^0 nanoparticles were obtained by reduction of $[CpRuCp^*RuCp^*]PF_6$ ($Cp^* = C_5Me_5$) with hydrogen and stabilized by the ionic liquid trihexyltetradecylphosphonium dodecylbenzenesulfonate [THTdP][DBS] [11]. The reduction of the iridium carborane, $(PPh_3)_2IrH(7,8\text{-}C_2B_9H_{11})$, with hydrogen in the presence of trihexyltetradecylphosphonium methylsulfonate, [THTdP][MS], produced Ir^0 nanoparticles. Both types of nanoparticles were used for catalytic applications. A facile synthesis of composite ruthenium-containing silica nanomaterials from amine stabilized-ruthenium nanoparticles $\{Ru@H_2N(CH_2)_nSi(OEt)_3\}$ as elemental bricks included the use of bifunctional $H_2N\text{–}(CH_2)_x\text{–}Si(OEt)_3$ amines as stabilizing ligands ($x = 3, 11$) for the synthesis of ruthenium nanoparticles, from [Ru(COD)(COT)] (COD = 1,3-cyclooctadiene, COT = 1,3,5-cyclooctatriene) as the metal precursor [12]. Resulting $[RuO_2]@SiO_2$ nanocomposites were found to possess a high specific surface area making them attractive materials for catalysis. Nanoparticles (5–10 nm) of $Ru_{1-x}Fe_x$ ($0 \le x \le 1$) in a carbon matrix were synthesized over the entire composition range using organometallic precursors of various molar mixtures (75:25, 50:50, 60:40, 75:25, and 95:5) of $Fe_2(CO)_9$:1,2,4,5-*tetrakis*(phenylethynyl)benzene and $Ru_3(CO)_{12}$:1,2,4,5-*tetrakis*(phenylethynyl)benzene [13]. In addition, multi-wall carbon

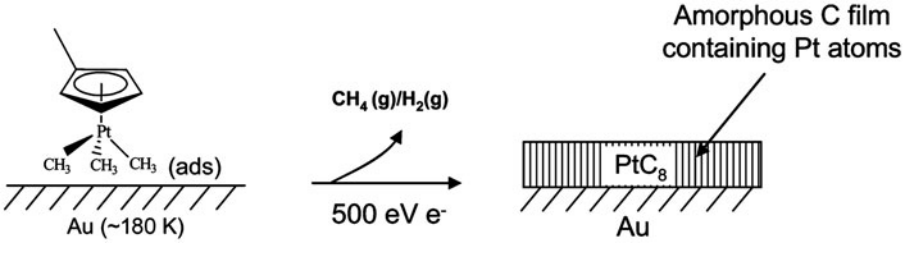

Figure 2. Electron induced reactions of adsorbed $MeCpPt^{IV}Me_3$.

nanotubes (MWCNTs) were formed during pyrolysis of these precursors. This is not uncommon, since carbon nanotubes are frequently formed from organometallics, such as, for example by pyrolysis of polyphenylene–cobalt complexes [14]. In case of gold complexes, electron beam (40–500 eV) induced reactions of $Au^{III}(acac)Me_2$ (**2**) adsorbed onto solid substrates were studied [15]. Electron irradiation of $Au^{III}(acac)Me_2$ was shown to be accompanied by reduction in Au^{III} to a metallic Au^0 species embedded in a dehydrogenated carbon matrix with the concomitant evolution of methane, ethane, carbon monoxide, and hydrogen (equation (2)). It was suggested that carbon removed as CH_4 or C_2H_6 from the $Au^{III}(acac)Me_2$ precursor were initially associated with the Au–CH_3 groups, while electron induced decomposition of the acac ligand can lead to evolution of carbon monoxide.

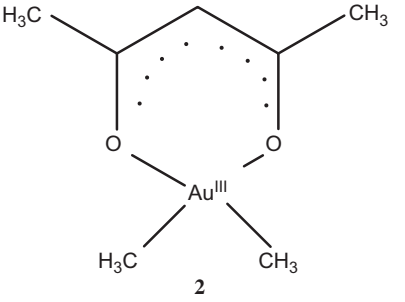

2

$$Au^{III}(acac)Me_{2(ads.)} + e^- \rightarrow Au^0C_6O_{0.8(s)} + H_{2(g)} + CH_{4(g)} + C_2H_{6(g)} + CO_{(g)} \qquad (2)$$

For transition metals, we note that mainly bimetallic compounds or more complex composites have been obtained from a variety of metal complexes containing the simplest and more sophisticated ligands, frequently from organometallics. Even classic N-containing Werner ligands were utilized for creation of their metal complexes with the goal of further decomposition and fabrication of nanostructures, for instance complexes containing ammonia as ligand. Thus, W–25% Cu nanocomposite was produced via a thermochemical co-precipitation procedure from copper nitrate and sodium tungstate salts as Cu and W containing precursors, respectively [16]. Aqueous solutions of these salts were reacted under controlled pH prepared by ammonia addition and the resulting precipitates were then calcined at 450 °C and hydrogen reduced at 800 °C. Using a basic medium with a pH of 13 which caused the formation of complex $[Cu(NH_3)_4]^{2+}$, it was found to provide suitable condition for precipitation of nanosized composite powders. As an example of P-containing ligands, polyphosphazenes containing anchored organometallic fragments are useful precursors for nanostructured metallic materials (an example **3** is organometallic derivative of the polyphosphazene with the anchored Mn-fragment) [17]. Pyrolysis in air at 800 °C yields metallic nanoparticles, $M^0/M_xO_y/M_z(P_xO_y)/P_4O_7$, depending on the metal used; i.e. M^0 when the metal is a noble metal; metal oxide when the metal is Cr, W, and Ru; metallic pyrophosphate when M=Mn and Fe. The organic spacer of the polyphosphazene influences strongly the morphology of the pyrolytic product. The mechanism of formation of the

nanostructured materials involves carbonization of the organic matter, which produces holes where the nanoparticles are grown. Reaction of the phosphorus polymeric chain with O_2 yield phosphorus oxide units, which act as a P_4O_7 matrix to stabilize the nanoparticles and/or $(P_xO_y)_n$ for the formation of metallic pyrophosphates.

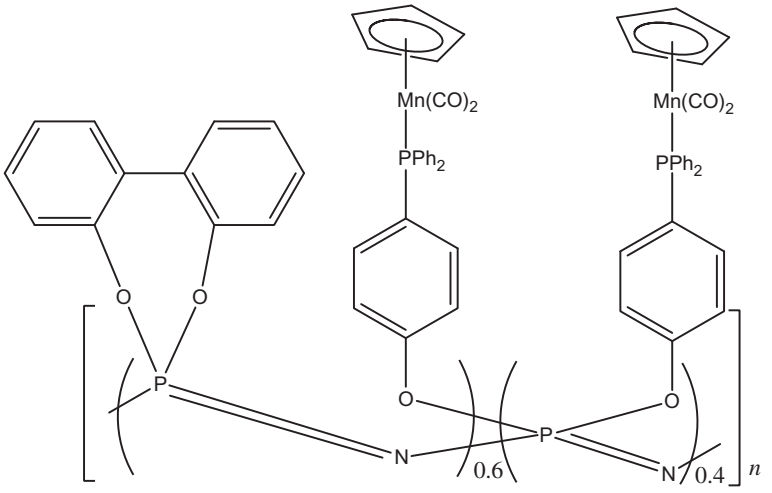

3

The synthesis of ultra-small iron(0) nanoparticles (6–10 nm) at moderate temperature – 120 to 150 °C – was carried out using the reduction of the iron(II) precursor $\{Fe[N(SiMe_3)_2]_2\}_2$ by HDA in the absence of dihydrogen (H_2) [18]. The nanoparticles are monodisperse in size and self-assemble into 2-D super-lattices suitable for transport measurements. Fe(II) reduction is accompanied by oxidation of amines into imines which were detected as by-products. Similarly, the one-pot reaction between *i*-$Pr_2NH{\cdot}BH_3$, $Rh(allyl)_3$, and $M[N(SiMe_3)_2]_2$ (M=Co or Fe) affords metal nanoparticles with a surface decorated with Rh (reaction 3) [19]. Classic β-diketonates, mainly acetylacetonates, are common in obtaining metal nanostructures (frequently bimetallic) on iron and nickel by different methods. For instance, Fe–Ni nanoparticles were synthesized via a non-aqueous solution-phase approach using thermal decomposition of Ni(II) acetylacetonate and Fe(III) acetylacetonate in oleylamine without further reducing agents [20]. The as-synthesized Fe–Ni nanoparticles possessed a face-centered cubic (fcc) crystalline structure and exhibited polydispersed and ferromagnetic characteristics. Related highly monodisperse 5 nm Pd–Ni alloy nanoparticles were prepared by reduction of $Pd(acac)_2/Ni(acac)_2$ mixtures with *t*-butylamine-borane complex in the presence of oleic acid (OA) and oleylamine (OAm) [21]. The Pd–Ni nanoparticles were well-dispersed on carbon supports and chemically dealloyed after acetic acid washing through selective dissolution of the less noble Ni component. The Pd–Ni catalysts exhibited much higher electrocatalytic activity and stability for ethanol oxidation than those of a commercial Pd/C catalyst. Titanium nitride (TiN)/nickel (Ni) composite coatings were synthesized [22] by plasma assisted metal–organic chemical vapor deposition (PAMOCVD) using dichloro-*bis*(η^5-cyclopentadienyl)titanium(IV) for titanium and N,N′-ethylene-*bis*(2,4-pentanedion-iminoato)nickel(II) for nickel. It was confirmed that Ni/TiN is a

nanocomposite coating containing nanocrystals of Ni and TiN with fcc structure; the films showed a uniform surface morphology.

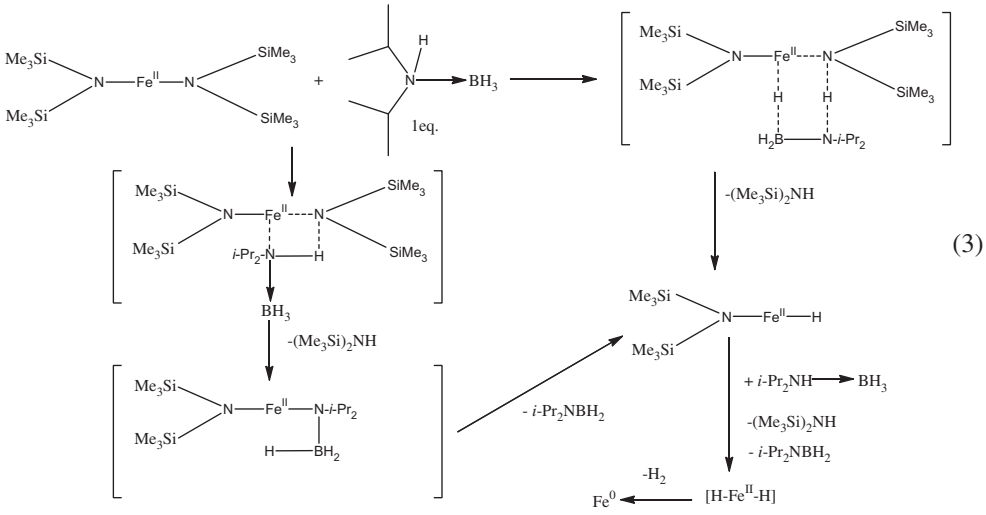

(3)

Mechanistic steps proposed for the reaction between the Fe amido complex and the amine-borane complex.

Among other bimetallic composites, we note a Sm–Co based nano-ferromagnetic material, synthesized by a Pechini-type sol–gel process, where a suitable gel precursor was prepared using respective metal salts and complexing agent such as citric acid (**4**) [23]. The gel precursor was dried at 300 °C and then subjected to various reductive annealing temperatures: 350, 500, and 600 °C. The binding of metal cations with the citrate molecules as metal-citrate complex was shown. The gel precursor, which was annealed at 350 °C, showed both meta-stable cobalt carbide (Co_2C, Co_3C) and Co_3O_4 phases, while the sample annealed at 500 °C indicated $SmCo_5$ phase. Intermetallic Fe–Sn and nanocrystalline metallic Sn nanoparticles were synthesized from organic precursors using the laser pyrolysis technique with ethylene as sensitizer [24]. Nano-Sn (single phase) was prepared by pyrolysis of $Sn(CH_3)_4$ (TMT) vapors. Controlled Fe/Sn atomic ratios ranging from 0.69 to 1.64 were obtained for the prepared Fe–Sn nanopowders by control of $Fe(CO)_5$ and TMT flows, respectively. Three main phases were detected: the tetragonal metallic Sn phase, the intermetallic $FeSn_2$ phase, and, to a much lesser extent, the cubic ternary carbide Fe_3SnC. The same products led to a completely different nanostructure in distinct conditions: iron(0) incorporated SnO_2 nanoparticles were generated [25] using an inverse coflow diffusion flame burner (figure 3) that supported a near-stoichiometric methane-air combustion. A liquid organometallic precursor solution of Sn $(CH_3)_4$ and $Fe(CO)_5$ was used to produce −1114 nm nanocrystalline particles. A flame temperature field was obtained to map particle evolution within the flame. The presence of elemental iron was confirmed, in particular, using inductively coupled plasma analysis yielding atomic ratio of 0.069 for Fe : Sn (2.2 at.% Fe in SnO_2 assuming stoichiometric oxygen content for tin).

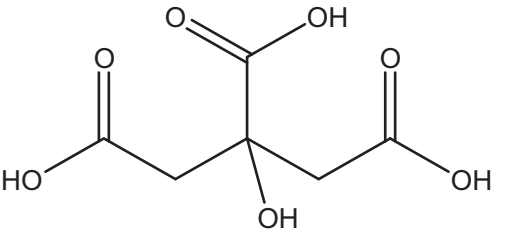

4

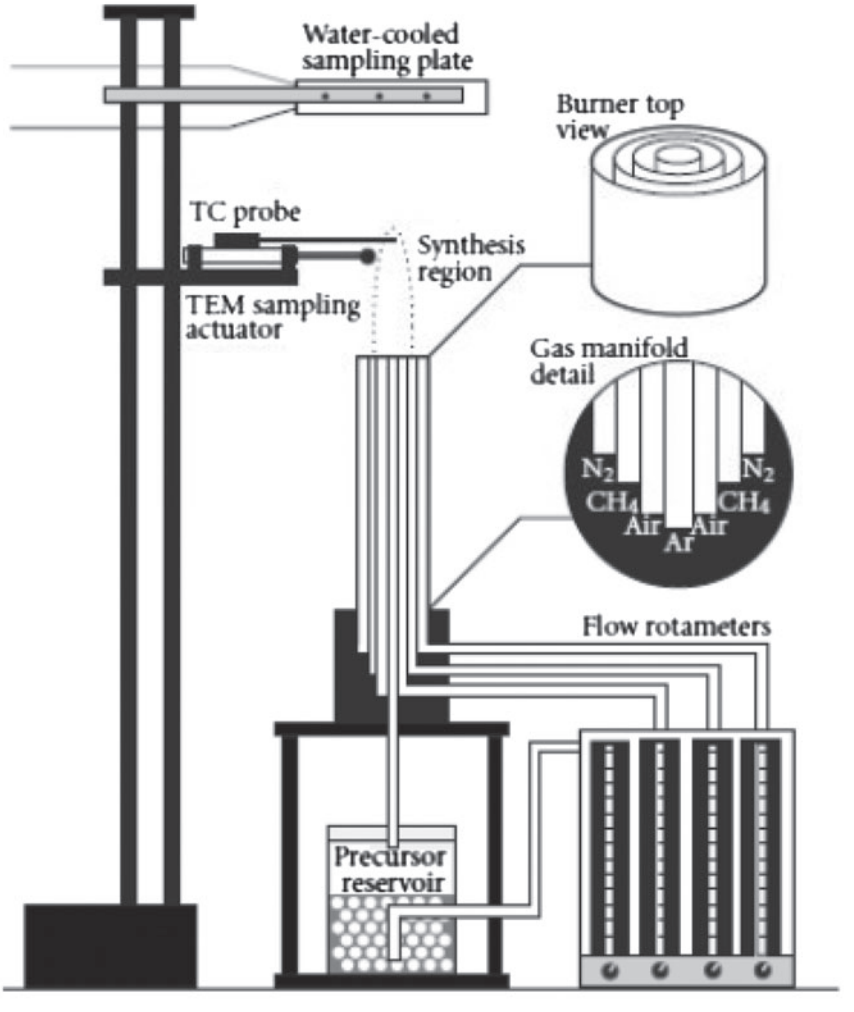

Figure 3. A custom-built bench-top coflow diffusion burner with premixed precursor delivery bubbler unit. Piston-cylinder actuator for TEM sampling and water-cooled bulk sampling plate for nanopowder collection.

To fabricate nanosized thin films, a series of homoleptic metal amidinates of the general type $[M(R\text{-}R'AMD)_n]_x$ (R = *i*-Pr, *t*-Bu, R′ = Me, *t*-Bu) was prepared and structurally characterized for Ti, V, Mn, Fe, Co, Ni, Cu (reaction scheme 4), Ag, Ru (reaction scheme 5), and La [26–28]. The chelating effect of the amidinate ligands contributes to the high thermal stability of the compounds. Despite this high thermal stability, the compounds are highly reactive, in part because the order of the metal–nitrogen bonds is only one-half. Their high reactivity under atomic layer ALD conditions was shown by the nearly complete removal of the ligands, which results in low impurity levels of the deposited films, as demonstrated in ALD of pure Fe, Co, Ni, Cu, Ru, FeO, CoO, and La_2O_3 thin films.

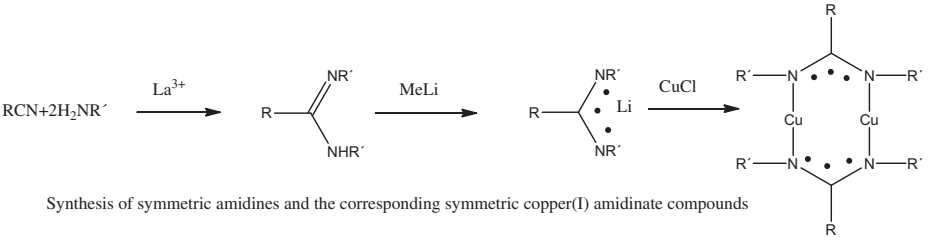

(4)

Synthesis of symmetric amidines and the corresponding symmetric copper(I) amidinate compounds

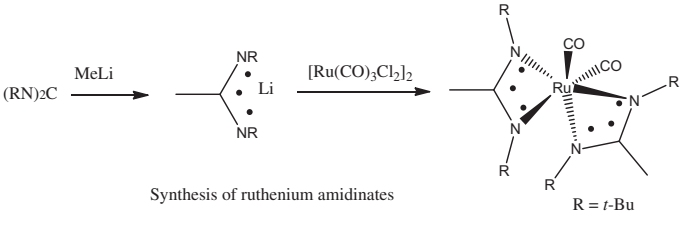

(5)

Synthesis of ruthenium amidinates

R = *t*-Bu

In addition to the methods above, a plasma-based scheme for preparation of ultrasmall (<5 nm in diameter) multimetallic nanoparticles was offered [29]. Nanoparticles were synthesized from vapors of classic organometallics such as *bis*(cyclopentadienyl) nickel(or iron) $[M^1(Cp)_2]$ or coordination compounds as copper or platinum acetylacetonate $[M^2(acac)_2]$. These MOCVD precursors were dissociated in plasma to homogeneously nucleate particles in the gas phase (figure 4). The obtained products are summarized in table 1. The process is potentially scalable, by operating large arrays of microplasmas in parallel, with low cost, and high purity, as it does not use surfactants to control particle nucleation and growth. Moreover, the method is generic, since there are many of these types of MOCVD precursors available, and should allow preparation of a wide range of multimetallic nanoparticles for applications as multifunctional materials.

Metal oxides and their composites

According to trends in nanotechnology, metal oxides are most used compounds in nanosize form. Among them, zinc oxide is the most popular, forming many classic and less-common nanostructures [30], so it is not surprising that a series of reports are dedicated to ZnO preparation from metal complexes with different N–, O–, N, O–, and N, S-containing ligands. Thus, formation of nanoscale zinc oxide particles with an almost

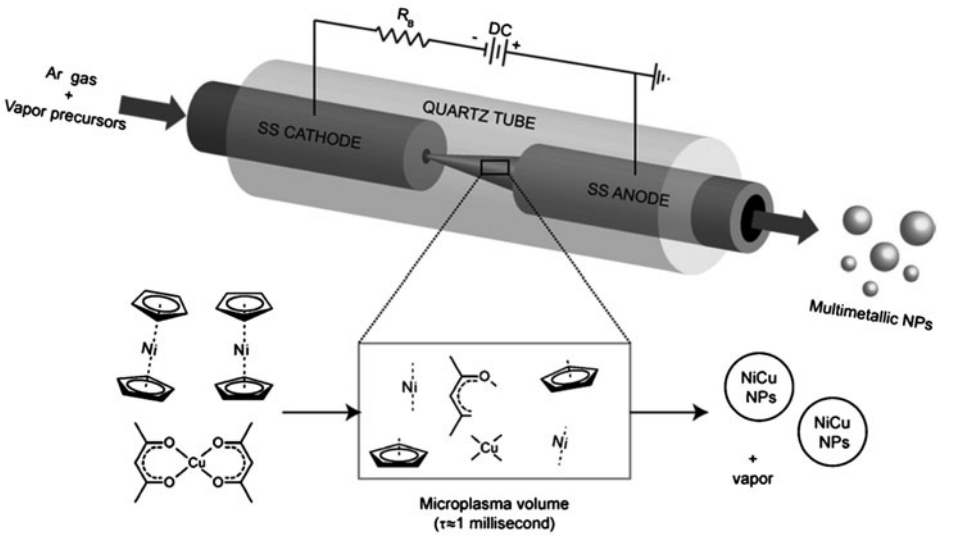

Figure 4. Schematic diagram of direct-current (dc), atmospheric-pressure microplasma reactor used to dissociate organometallic vapors and continuously synthesize multimetallic nanoparticles. A hypothesized mechanism for formation of NiCu bimetallic nanoparticles is also shown. Vapor precursors are dissociated in the plasma volume (τ is the residence time) to form radical moieties that nucleate multimetallic NPs.

Table 1. Summary of aerosol measurements for mono-, bi-, and tri-metallic nanoparticles synthesized in plasma reactor from various coordination and organometallic compounds.

Nanoparticles	Metal precursor	Vapor pressure	Metal precursor flow rate (sccm)	D_{pg}	σ_g
Ni	$NiCp_2$	13 torr	20	3.5	1.15
		293 K[a]	15	3.3	1.13
			10	2.8	1.07
Fe	$FeCp_2$	13 torr	20	4.7	1.22
		293 K[a]	15	4.2	1.19
			10	3.8	1.16
Cu	$Cu(acac)_2$	14 torr	30	5.9	1.30
		383 K[b]	20	3.9	1.19
			10	3.2	1.12
Pt	$Pt(acac)_2$	500 torr	20	3.5	1.19
		455 K[c]	10	2.7	1.09
$Ni_{0.47}Cu_{0.53}$			10 + 10	3.9	1.18
			7.5 + 7.5	3.6	1.15
			5 + 5	3.2	1.12
$Ni_{0.18}Cu_{0.82}$			5 + 20	5.3	1.30
			4 + 16	4.5	1.25
$Ni_{0.22}Fe_{0.29}Cu_{0.49}$			7.5 + 7.5 + 15	4.8	1.25
			5 + 5 + 10	3.7	1.16
$Ni_{0.342}Fe_{0.46}Cu_{0.20}$			10 + 10 + 5	4.5	1.21

[a]Ni and Fe precursors were sublimed at r.t.
[b]Cu precursor was sublimed at 383 K.
[c]Pt precursor was sublimed at 373 K.
Abbreviations: geometric mean particle diameter (D_{pg}) and geometric standard deviation (σ_g).

monomodal size distribution by microwave heating of solutions of mononuclear zinc oximato or zinc acetylacetonato complexes in various alkoxyethanols was investigated [31]. Field-effect transistor devices with these ZnO particles as the active semiconducting layer exhibited a charge carrier mobility of 0.045 $cm^2/(V\ s)$ and I on/off current ratios of ~460.000, with a threshold voltage of 8.78 V. The rapid and massive formation of a foamy precipitate while reacting zinc acetate and triethanolamine (TEA) in proper conditions led to an unraveled complex and a molecular tetra-metallic zinc cluster [32], whose structure shows the direct link of the acetate to the Zn cation, a feature not observed in parent compounds. This cluster structure can be considered an interesting precursor for zinc oxide as nano-aggregates of four ZnO moieties are already present and the formation of ZnO particles requires a smaller number of broken and newly formed bonds. Zinc(II) 2-oximinopropionate dihydrate $[Zn(PAO)_2(H_2O)_2]$ was precipitated by treatment of an aqueous solution of zinc sulfate with sodium pyruvate oxime, $Na(PAO)\cdot H_2O$ [33]. Its stepwise decomposition also led to zincite ZnO.

The host and the apohost framework of $[Zn_2(1,4\text{-bdc})_2(dabco)]\cdot 4DMF\cdot 0.5H_2O$ (1,4-bdc = 1,4-benzenedicarboxylate and dabco = 1,4-diazabicyclo[2.2.2]octane) were used [34] for preparation of ZnO nanomaterials. With calcination of the host framework of this complex, ZnO nanoparticles could be fabricated. However, by the same process on fully desolvated framework of this compound, ZnO microrods composed of ZnO nanoparticles were formed (reaction 6). It was concluded that the role of guest DMF in preparation of ZnO nanoparticles from the solvated complex is similar to the role of polymer stabilizers in the formation of nanoparticles. The same authors used 4′-(4-pyridyl)-2,2′:6′,2″-terpyridine (pyterpy) as a ligand for preparing three zinc(II) coordination polymers, $[Zn(pyterpy)(OAc)]ClO_4$, $[Zn(pyterpy)I_2]$, and $[Zn(pyterpy)_2](ClO_4)_2(H_2O)_{2.9}$ (pyterpy **5**). The first two coordination polymers were synthesized by slow evaporation while the last was prepared through hydrothermal method. Pure phase ZnO nanoparticles with different sizes and morphologies were obtained by direct calcination of each complex [35]. Also, metal N, O-containing complexes can be used for obtaining doped nanoparticles. For example, an unusual square pyramid Mn(III) complex, $[Mn(L)(H_2L)]PF_6$, where L = (5,5′-dimethoxy-2,2′-(propane-1,2-diyl-*bis*(nitrilomethylidyne))diphenolato), crystallized in monoclinic with space group P_21/n, was applied as a precursor for synthesis of Mn-doped ZnO nanoparticles [36]. The Mn is coordinated with L (Schiff base) as N_2O_2 tetradentate ligand in the equatorial position and H_2L as O monodentate in axial position.

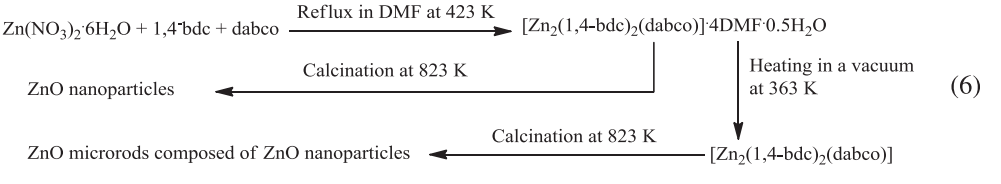

(6)

Decomposition of $[Zn_2(1,4\text{-bdc})_2(dabco)]\cdot 4DMF\cdot 0.5H_2O$ in various conditions

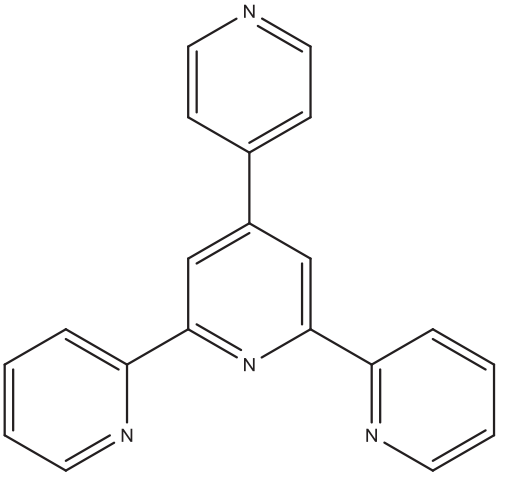

5

N, S-containing ligands have been used not only to prepare metal sulfide nanoparticles, as expected, but also metal oxides, more thermodynamically stable in air. Thus, nanoparticles of a Zn(II) coordination polymer, $\{[Zn(DADMBTZ)(CH_3COO)_2]_n\}$ (DADMBTZ = 2,2′-diamino-5,5′-dimethyl-4,4′-bithiazole **6**; see also the section on metal sulfides), were synthesized by reaction of $Zn(NO_3)_2{\cdot}4H_2O$, CH_3COONH_4 and DADMBTZ by a sonochemical method. In this four-coordinate compound with nearly C_2 symmetry, DADMBTZ is bidentate. The metal lies in a pseudotetrahedral environment and is ligated by the two bithiazole ring nitrogens and oxygen from each of the two monodentate acetates; 2-D networks are formed via N–H– – –O hydrogen bonds. A ZnO nanostructure was obtained by direct thermolysis at 500 °C under air (scheme 7) [37]. The same ligand was used for obtaining Co_3O_4 nanoparticles. Thus, nano-scale and single crystals of a related azido Co(II) complex $\{[Co(DADMBTZ)_2(N_3)_2]$ $0.25CH_3OH\}$ were synthesized [38] by the reaction of cobalt chloride, sodium azide, and DADMBTZ using sonochemical and heat gradient methods, respectively. The coordination number of cobalt in the compound was six with distorted octahedral, CoN_6. Co_3O_4 nanostructures (see also below in this section) were obtained by direct thermolysis of this at 450 °C under air. In addition, the synthesis of nanostructured (38–54 nm) Zn(II) complex of cysteine (**7**) $[ZnI_2(C_3H_5NO_2S)]_n$ (cysteine = 2-amino-3-mercaptopropanoic acid) was carried out by reaction (8) of zinc(II) acetate and KI with cysteine under ultrasonic irradiation [39]. The hexagonal microcrystalline zinc oxide was then prepared using Zn(II) cysteine complex as precursor by calcination at 600 °C for 2 h.

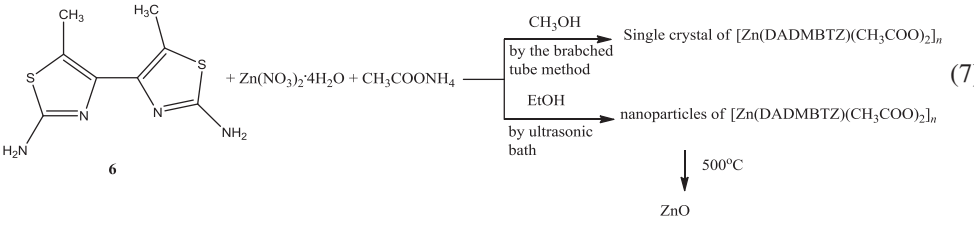

(7)

Preparation of ZnO nanoparticles from $[Zn(DADMBTZ)(CH_3COO)_2]_n$.

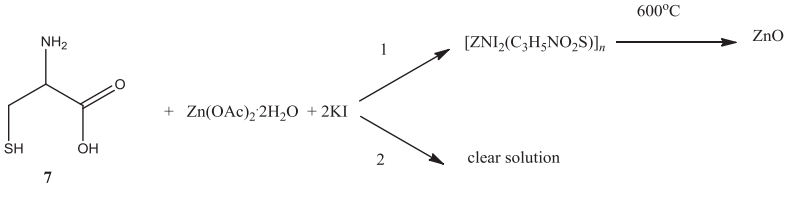

(8)

1: UNDER ULTRASONIC IRRADIATION
2: BRANCHED TUBE TECHNIQUE, ABSENCE OF ULTRASONIC IRRADIATION

Nanoparticles of a 3-D supramolecular Cd(II) compound, $[Cd(L)_2(H_2O)_2]$ (L^- = 1H-1,2,4-triazole-3-carboxylate, **8**), were synthesized by a sonochemical process [40]. Its calcination at 650 °C under air yielded CdO nanoparticles. An aza-aromatic base adduct of cadmium(II) thenoyltrifluoroacetonate, $[Cd(phen)(ttfa)_2]$ (phen = 1,10-phenanthroline; ttfa = thenoyltrifluoroacetone **9**), was synthesized [41]. It was shown that the coordination number of the Cd^{2+} ions is six with two nitrogen donors from aza-aromatic base ligands and four oxygen donors from two thenoyltrifluoroacetonates. The CdO nanoparticles (45 nm) were obtained by thermolysis of this complex at 180 °C with oleic acid as a surfactant. We emphasize that as a result of this reaction CdO nanoparticles are formed, in comparison with CdS formation from Cd/S-ligand complexes in the majority of the reactions below (see section on metal sulfides).

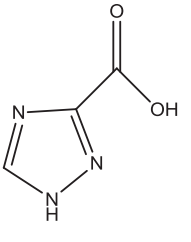

8

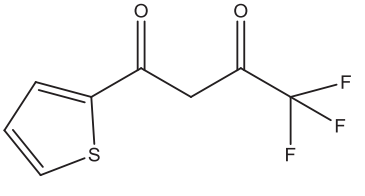

9

Among O-containing ligands, simple and oxo-acetates, as well as oxalates, have been frequently used as precursors for obtaining nanostructural metal oxides of distinct dimensionality. Thus, uniform mesocrystalline 1-D MnO nanorods (figure 5), exhibiting uniform morphology, large specific surface area, and narrow pore size distribution, were prepared [42] by using manganese acetate and ethanol as starting materials in solvothermal conditions at 200 °C for 24 h under N_2 in the absence of polymer additives. Their possible formation mechanism is presented in figure 6. Owing to their large specific surface area

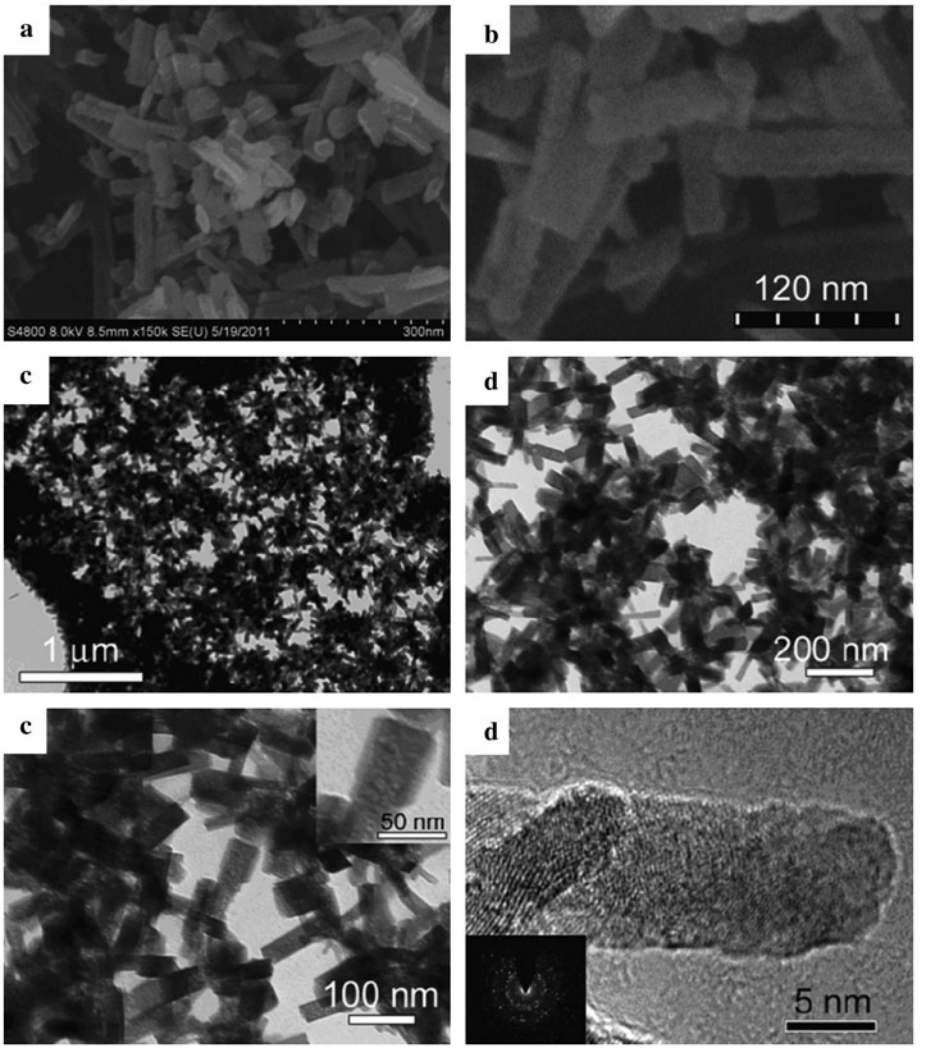

Figure 5. Morphology of the cubic MnO nanorods obtained at 200 °C for 24 h. (a) Low-magnification and (b) high-magnification SEM images, ((c), (d), and (e)) TEM, and (f) HRTEM images. The inset in (e) is an enlarged TEM image and the inset in (f) shows the SAED pattern of one single MnO nanorod.

(153 m^2/g), the as-prepared MnO nanorods may have promising applications in energy storage, catalysis, and biomedical imaging. Crystal growth of cobalt(II) oxalate in silica gel at r.t. as precursor of Co_3O_4 nanoparticles was studied [43]. Two different reaction tube types (figure 7) were used toward crystallization of cobalt(II) oxalate in gel, which was prepared at pH 5 by reacting sodium metasilicate solution with dilute nitric acid (U-tube) and oxalic acid (straight tube), with gelling time of 4 days and crystal growth time of 8 (for straight tube) and 12 (for U-tube) weeks. We note that currently high demand of cobalt(II) oxalate as precursor of multi-functional materials of Co_3O_4 is observed.

A series of reports is devoted to nickel oxide nanostructures. Thus, NiO nanofibers consisting of nanograins were synthesized by an electrospinning method with polyvinyl

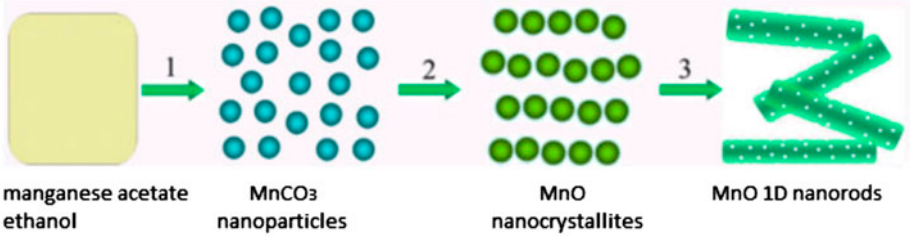

Figure 6. The possible formation mechanism of the MnO 1-D nanorods.

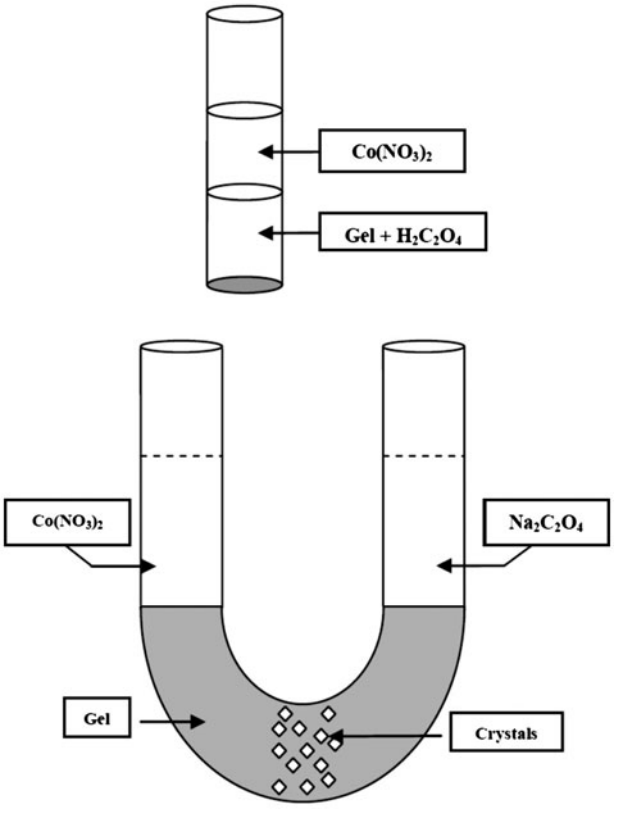

Figure 7. Reaction scheme of straight tube (top) and U-tube (bottom) method.

alcohol and nickel acetate tetrahydrate as precursor materials [44]. On the basis of the obtained product, a gas sensor was fabricated showing good sensing properties to NO_2 and benzene. The Ni(II) complexes $[Ni(L)_2](ClO_4)_2$ and $[Ni(L)_2(NO_3)_2]$, where L is the Schiff base 4,5,9,13,14-pentaaza-benzo[b]triphenylene, were synthesized and used for obtaining NiO nanoparticles by calcination at 500 °C [45]. The free Schiff base and its Ni(II) complexes were screened for antibacterial activities against three Gram-positive bacteria,

showing that the metal complexes are more active than the free Schiff base. Nanoparticles of a Ni(II) metal–organic framework with cubic building blocks and 1-D open channels, i.e. $\{[Na_{16}(Ni_8L_{12})(H_2O)_{20}(H_2O)_4](CH_3CN)(H_2O)_{18.5}\}_\infty$ (H_3L = 4,5-imidazoledicarboxylic acid, **10**), were synthesized by using ultrasonic method [46]. Calcination of the bulk powder and nano-sized compound at 700 °C under air yielded NiO nanoparticles with size and morphology of the NiO nano-particles dependent upon the particle size of the initial compound.

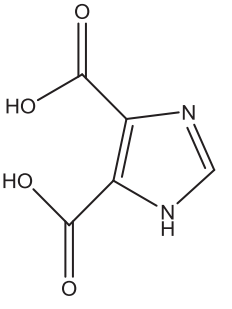

10

Various iron oxides were produced as nanostructures. Thus, a Fe(II) 1-D coordination polymer, $[Fe(pyterpy)_2](SCN)_2 \cdot MeOH$ (pyterpy is **5**), was synthesized by using a branched tube [47]. Iron(III) oxide nano-particles were obtained by thermolysis of this compound in oleic acid (surfactant) at 286 °C under air. Classic ferrocene $Fe(C_5H_5)_2$ can be used as a precursor for synthesis of carbon-coated α-Fe_2O_3 nano-particles [48]. The pyrolysis of ferrocene leads to formation of a compound that can be fully converted into carbon-coated α-Fe_2O_3 nano-particles (50–100 nm) via simple oxidation in air. Varying the oxidation temperature, it is possible to control precisely the carbon coating on the nano-particles. For comparison, in different conditions, aligned carbon nanotubes were synthesized [49, 50] by microwave irradiation heating from ferrocene (figures 8 and 9). CNTs contain a metal particle at the tip of each tube. This carbon nanostructure promises to become important in fuel cells and in nanoscale engineering of other systems in which electrical effects, mechanical, and chemical interactions are integrated to produce macroscale. In case of Fe_3O_4, its water-soluble nanopowder with mesoporous structure was prepared by thermal decomposition of Fe–urea complex $\{[Fe(NH_2CONH_2)_6](NO_3)_3\}$ in triethylene glycol (TEG) [51]. It was established that prolonging reflux time and increase in concentration of $\{[Fe(NH_2CONH_2)_6](NO_3)_3$ in TEG can improve the crystallinity and magnetic properties of the Fe_3O_4 nanopowder. The saturation magnetization (Ms) increased from 21.4 to 48.5 emu/g when the reflux time increased from 2 to 20 h. The maximum adsorption capacity of the Fe_3O_4 nanopowder for Cr(VI) was estimated to be 21.6 mg/g. It is known that nano zero-valent iron (NZVI) and its nanostructured oxides remediate Cr(VI) and As(V) from the environment [52].

As well as zinc oxide, copper oxides (mainly CuO) are frequently obtained from copper complexes containing a variety of ligands with N–, O–, and P-donors. Thus, submicron- and nano-scale cuprous oxide (Cu_2O) particles derived from copper acetate and copper gluconate complexes were synthesized [54] via a photochemical route in polar media without further reducing agents. Solvent is the key factor in size-control and shape-control of the Cu_2O products: water induces formation of submicron particles, while alcohol results in

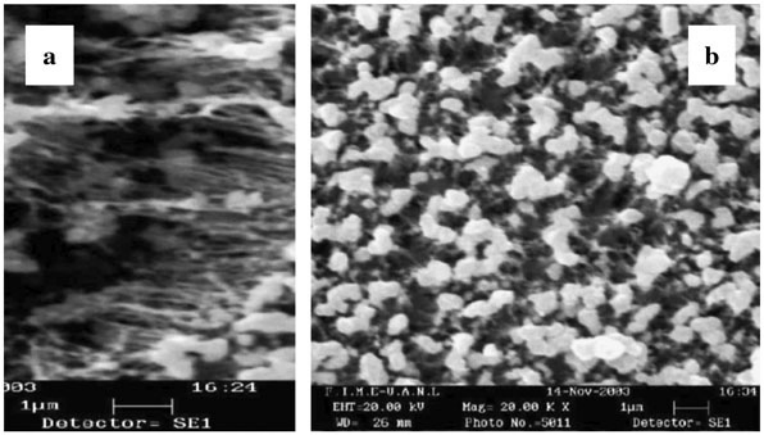

Figure 8. SEM images of vertically aligned nanotubes obtained by MW-heating of ferrocene for 30 min: (a) high-magnification view of the bottom-end of the array; (b) high-magnification view of the inclined vertically aligned nanotubes.

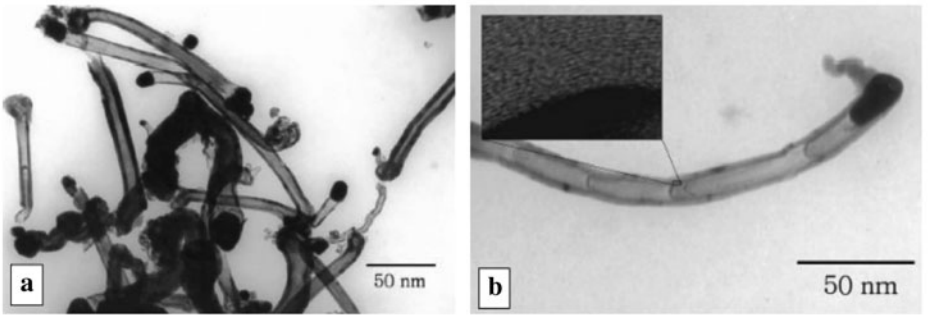

Figure 9. (a) TEM images of an Fe-filled CNTs grown by microwave heating for 20 min; (b) straight nanotube with bamboo compartments grown by microwave heating for 20 min [53].

nanoscale particles. The photochemical growth of Cu_2O particles can be fine tuned by varying the parameters of the reaction procedure, e.g. solvent, precursor ligand, and additive. In addition, Cu_2O particles result from photoinduced intramolecular electron transfer between metal and ligand. The method can be easily controlled and is expected to be applicable for the preparation of cuprous oxide supported catalysts.

A nanosized copper(II) supramolecular compound, $[Cu(dipic)(H_2O)_2]_n$ [dipic = 2,6-pyridinedicarboxylate], was synthesized by sonochemical method (scheme 9) [55]. The nanorod copper(II) supramolecular compound adopts a 3-D supramolecular network owing to extensive hydrogen-bonding and π–π stacking. Calcination of this nanosized compound at 500 °C under air yielded CuO nanoparticles. Also, spongy CuO (average diameter altering from 10 to 20 µm) was synthesized [56] via direct pyrolysis of $Cu_3(btc)_2$ (btc = benzene-1,3,5-tricarboxylate) microporous metal–organic framework in a horizontal tube furnace in air, in which

$Cu_3(btc)_2$ was used as the Cu source and complexing molecule precursor. The reaction temperature played a key role in formation of spongy CuO microstructures. The product consisted of nanosheets with average edge length of 80–200 nm and thickness of about 30 nm. This spongy material could find application in catalysis, absorption, and gas sensing.

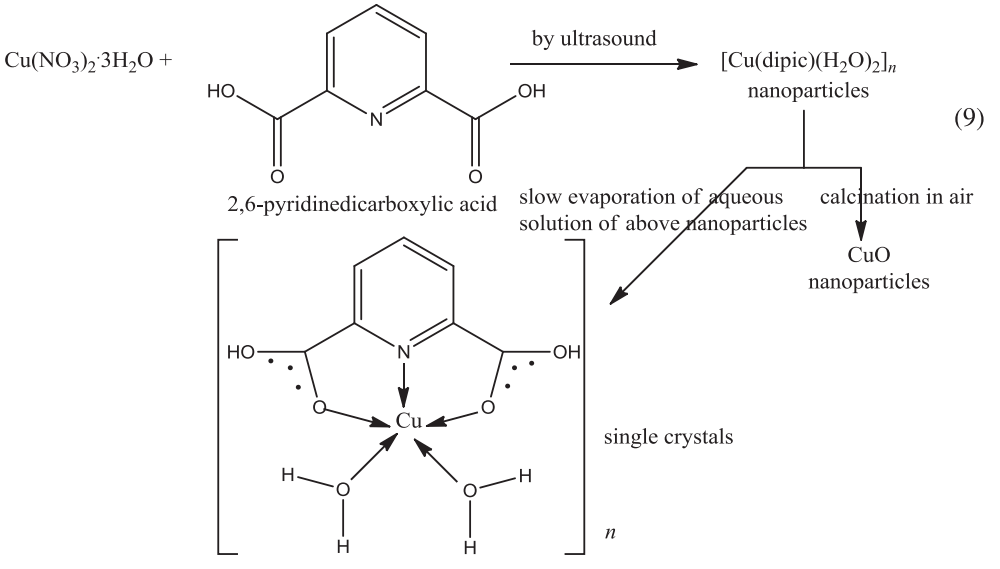

The complexes with "pure" N-containing ligands (such as, for example **5**), applied for nanoparticle formation, are rare, and their one example corresponds precisely to preparation of CuO in classic nanorod and less-common nanoflower structures. Thus, the rod-like (about 50 nm in diameter and up to 500–700 nm in length) and dandelion-like (average diameter of 2 μm) CuO nanomaterials were prepared by decomposition of $[Cu(pbbt)Cl_2]_2 \cdot CH_3OH$ {pbbt = 1,1′-(1,3-propylene)-*bis*-1H-benzotriazole} in the presence of surfactants and alkalies under hydrothermal conditions [57]. The sensitivity to gasses of the as-prepared CuO nanorods was better than that of dandelion-like CuO particles, and the CuO nanorods displayed special sensitivity to alcohol. Finally, the thermal atomic layer deposition of copper oxide films from non-fluorinated liquid precursor *bis*(tri-*n*-butylphosphane)copper(I) acetylacetonate **11**, [(*n*-$Bu_3P)_2$Cu(acac)], and wet O_2 on Ta, TaN, Ru, and SiO_2 substrates at 100–160 °C was reported [58]. Precursor self-decomposition in a chemical vapor deposition mode led to bimodal growth on Ta, resulting in parallel formation of continuous films and isolated clusters. This effect was not observed on TaN up to 130 °C and neither on Ru or SiO_2 for any processing temperature. Being nonfluorinated, the Cu precursor avoids a major source of adhesion problems well known from Cu CVD; another advantage is that the precursor is a liquid under standard conditions and can be stored in an inert gas atmosphere for months without decomposition. This is another important fact for practical applications as solid source precursors are prone to particle generation during deposition. The results are a promising basis for Cu seed atomic layer deposition applicable to electrochemical Cu metallization in interconnects of ultra-large-scale integrated circuits.

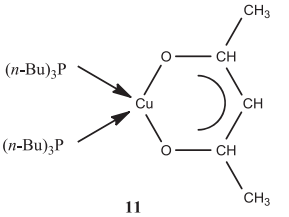

11

Complexes of various Schiff bases and related ligands can also be precursors for nanoparticles of oxides of copper and other metals. Thus, a symmetric tetradentate Schiff base ligand, N,N′-*bis*(5-bromosalicylaldehyde)-1,3-phenylenediamine [$(Brsal)_2$-1,3-phen), **12**], and its Cu(II) and Co(II) complexes (**13**) with general formula $M_2((Brsal)_2$-1,3-phen$)_2$, where M=Co and Cu], were synthesized (reaction 10) and used as precursors for corresponding metal oxide nanoparticles [59]. Cu(II), Co(II), and Ni(II) complexes {$[Cu(H_2L)(H_2O)_2(Cl)]Cl$, $[Co(H_2L)(H_2O)_3]Cl_2{\cdot}3H_2O$ and $[Ni(H_2L)(H_2O)_2]Cl_2{\cdot}6H_2O$} were synthesized from 2-[(5-*o*-chlorophenylazo-2-hydroxybenzylidin)amino]-phenol Schiff base (H_2L) [60]. Metal ions coordinate tetradentate or hexadentate with this O_2N-donor ligand (metal–ligand stoichiometry is 1 : 1). Preparation of single phases of CuO, CoO, and NiO nanoparticles using these H_2L complexes as precursors via a solid-state decomposition procedure was carried out.

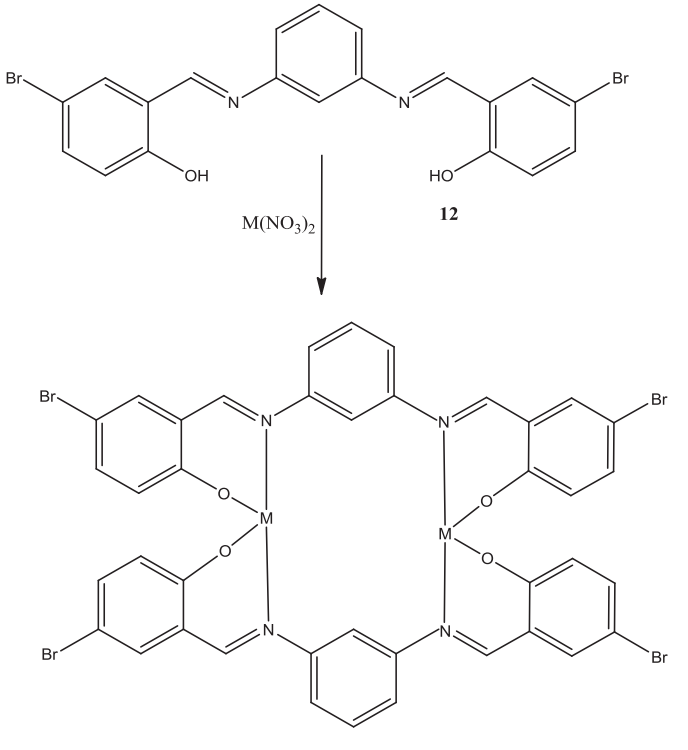

12

13

(10)

The chemical structure of ligand 12 and its complexes 13 with Co(II) and Cu(II).

Titanium dioxide TiO_2 nanopowder, another "heart" of the nanotechnology together with ZnO, carbon nanotubes and graphene, was prepared by a green approach by solution combustion using titanium peroxo complex and tartaric acid (TA) as an initial precursor [61]. The water-soluble peroxo-α-hydroxy-carboxylato titanium complex, an intermediate precursor mass at external temperature of 500 °C, resulted in the oxide of pure anatase phase. Nanopowders of TiO_2 were also prepared by a microwave irradiation-assisted route, starting from *bis*(ethyl-3-oxo-butanoato)oxotitanium(IV), $[TiO(etob)_2]_2$, as precursor and polyvinylpyrrolidone (PVP) as a capping agent [62]. It was suggested that a unique step of initiation of transformation takes place in $Ti_{1/2}O$ layers in anatase. Interaction products of Ti(OPr-*i*)$_4$ with HOSi(O-*t*-Bu)$_3$ and further reactions with glycols were studied [63]. In particular, it was established that hydrolysis of the glycol modified derivative, $[Ti(OPr\text{-}i)(O\text{-}(CH_2)_2\text{-}O)\{OSi(O\text{-}t\text{-}Bu)_3\}]$, by sol–gel technique affords the homogenous titania–silica material $TiO_2{\cdot}SiO_2$ in nano-size, while the precursor $[Ti(OPr\text{-}i)_3\{OSi(O\text{-}t\text{-}Bu)_3\}]$ yielded a nonstoichiometric silica doped titania material. However, pyrolysis of $[Ti(OPr\text{-}i)_3\{OSi(O\text{-}t\text{-}Bu)_3\}]$ yielded nano-sized crystallites of $TiO_2{\cdot}SiO_2$.

An analog of titanium dioxide, ZrO_2 in different forms is also an object of investigations; the difference between them is that mainly organometallics have been applied to synthesize ZrO_2. Thus, a synthetic strategy based on combination of the chlorination of an organometallic precursor ($ZrCp_2Cl_2$) followed by solvothermal treatment was found to be successful in synthesis of tetragonal nano-ZrO_2 or nano-ZrO_2 embedded in an amorphous carbon matrix, depending on the solvent employed in the solvothermal step (figure 10) [64]. The formed nanoparticles consist of tetragonal ZrO_2 with average sizes of 1.7 ± 0.4 and 6.2 ± 0.9 nm for the embedded in carbon and the free nano-ZrO_2, respectively. Some volatile *bis*-cyclopentadienyl zirconium alkoxides, $Cp_2Zr(OR)(O\text{-}t\text{-}Bu)$ (R = *i*-Pr, Et, Me), were synthesized by reaction of the corresponding KOR with the intermediate $Cp_2ZrCl(O\text{-}t\text{-}Bu)$ [65] and then used for depositing zirconia thin films of high quality and purity on Si(100) and stainless steel AISI 316 substrates by metal–organic MOCVD.

Nanocrystalline α-Al_2O_3 powders were prepared [66] by pyrolysis of aluminum acetylacetonate. The optimum calcination temperature of the precursor powder for crystallization of nano α-Al_2O_3 was 1000 °C for 2 h. It was shown that the obtained materials could be modified from segregated nanoparticle to aggregates of nanoparticle with decrease in the

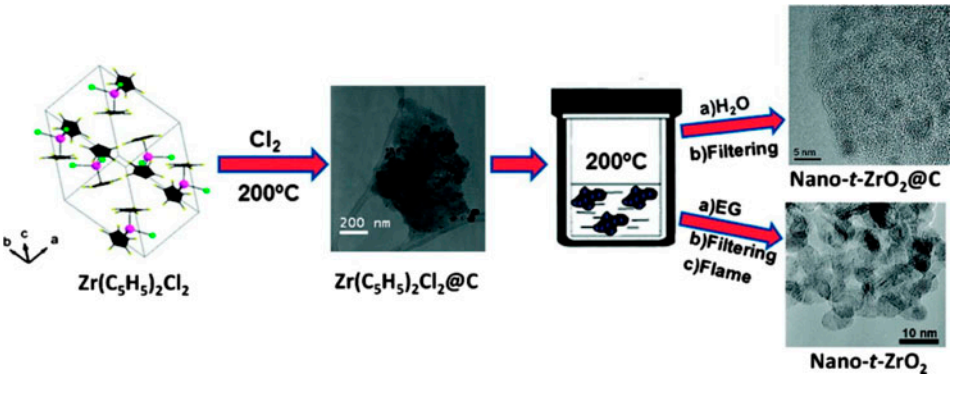

Figure 10. Schematic representation of the synthetic procedure followed in the synthesis of nanometric ZrO_2. On the left, a unit cell of the $Zr(C_5H_5)_2Cl_2$ precursor is drawn.

volume ratio of alumina to acetylacetone from 8:2 to 5:5 in the precursor solutions. Another example is ultra-fine α-alumina fibers, prepared via electrospinning technique (figures 11 and 12) using PVP polymer solution and aluminum isopropoxide/aluminum acetate as alumina precursors followed by calcinations at higher temperature [67]. The crystalline phase and fiber morphology were influenced by calcination temperature. In case of the alumina analog, indium(III) oxide, a porous indium(III) metal–organic framework, $[In_2(OH)_2(C_{10}O_8H_2)]_n \cdot 2nH_2O$ (MIL-60, $C_{10}O_8H_2$ = 1,2,4,5-benzenetetracarboxylate), was synthesized [68] by hydrothermal method and used for preparation of In_2O_3 nanoparticles by direct thermal decomposition of MIL-60 at 450 °C under air.

A series of lead-containing complexes have been applied for PbO nanoparticle formation. PbO nanoparticles serve as catalyst [69] for multicomponent organic synthesis reactions, for instance Paal–Knorr reaction and oxidative coupling of methane, due to the significant catalytic property with operational simplicity, high reactivity, environmental friendliness, reduction of reaction times, and reusability of PbO nanoparticles [70]. In this respect, a

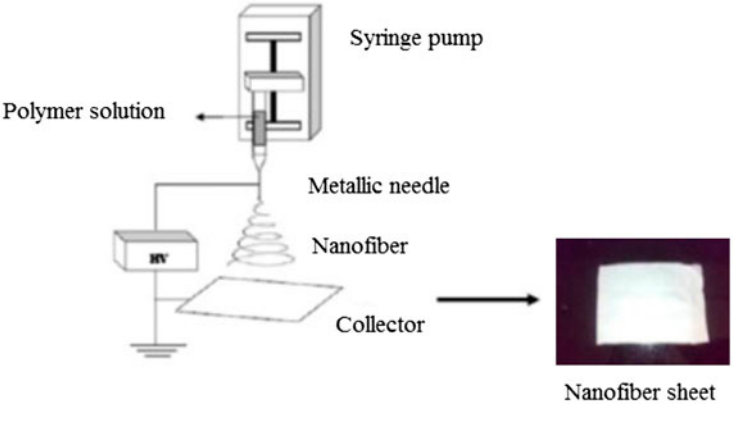

Figure 11. Schematic diagram of electrospinning setup.

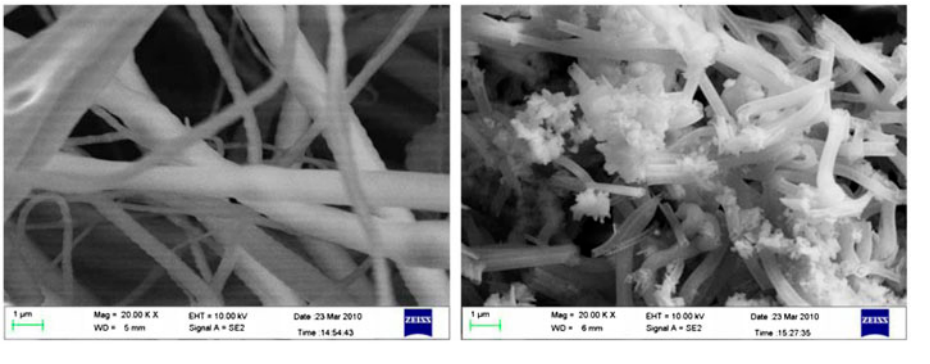

Figure 12. FESEM images of as spun nanofiber of (a) PVP-aluminum *iso*propoxide precursor and (b) sintered at 1000 °C.

coordination polymer of lead(II) nitrate complexes with bridging *trans*-1,2-*bis*(4-pyridyl) ethene (bpe) ligand, $[Pb(\mu\text{-}NO_3)_2(bpe)(MeOH)]_n$, was used [71] to prepare PbO nano-particles using two different methods. In this compound, lead(II) ions are bridged by nitrates forming linear chains, which are further coordinated by neutral bpe and methanol into a 2-D polymeric chain. Also, nanoparticles of a Pb^{II} metal–organic polymer, $[Pb(\mu\text{-pyr})(\mu\text{-}I)_2]_n$, with a net-like morphology were synthesized [72] by reaction of pyrazine **12** with $Pb(NO_3)_2$ and NaI via sonochemical irradiation. Nano-structured PbI_2 and PbO were synthesized from this complex by calcination with argon and air, respectively. Nanostructures (50 nm) of Pb(II) 2-D coordination polymers, $[Pb_2(\mu_2\text{-bpdbe})_2(NO_3)_4]_n$ {2-bpdbe = 1,6-*bis* (2-pyridyl)-2,5-diaza-1,5-hexadiene}, were synthesized by the sonochemical method [73]. This structure may be considered a coordination polymer of lead(II) formed by bridging 2-bpdbe ligands, making a 2-D array of $Pb(NO_3)_2$ and 2-bpdbe. Its thermolysis in oleic acid as a surfactant at 180 and 200 °C under air led to PbO particles about 60 nm. In addition, preparation of plate-shaped nanostructures of a 1-D polymeric lead(II) complex containing the $Pb_2\text{-}(\mu\text{-}I)_2$ motif, $[Pb(neo)I_2]_n$ {neo = neocuproine or 2,9-dimethyl-1,10-phenanthroline (dmp), **13**}, using a sonochemical method was described [74]. A coordination number of six is for Pb^{II} (i.e. PbN_2I_4) with an asymmetrical coordination sphere and "stereo-chemically active" electron lone pairs. PbO nanoparticles (~25 nm) are obtained by thermolysis of this compound at 180 °C with oleic acid as a surfactant. Similarly, $[Pb_2(dmp)_2(\mu\text{-}N_3)_2(\mu\text{-}ClO_4)_2]_n$ [75] and $[Cd(dmp)(ttfa)_2]_n$ (ttfa = thenoyltrifluoroacetonate) [76] were prepared and used for PbO and CdO nanoparticles preparation, respectively. The lead complex has a "stereo-chemically active" electron lone pair, and the coordination sphere is hemidirected. The supramolecular features in these complexes are controlled by weak directional intermolecular interactions. The chains interact with each other through π–π stacking interactions creating a 3-D framework.

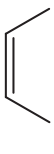

12

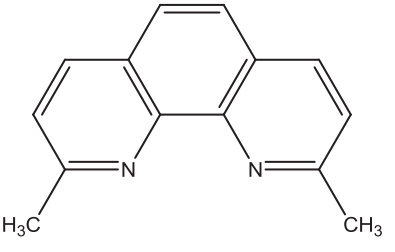

13

Different N-heterocyclic ligands with carboxyl or carboxamide groups have also been used. Thus, nanobelts of a lead(II) coordination polymer, $[Pb(3\text{-}pyc)_2]_n$, 3-Hpyc = 3-pyridinecarboxylic acid (**14**), were synthesized by a sonochemical method [77]. After calcination at 400 °C, pure phase nano-sized lead(II) oxide was produced. A Pb(II) complex, $\{[Pb_2(tpmba)_2(NO_3)_4]\cdot MeOH\}_n$, was obtained [78] by reaction of a tripodal ligand, N,N′,N″-*tris*(pyrid-3-ylmethyl)-1,3,5-benzenetricarboxamide (tpmba), with Pb $(NO_3)_2$. Structural analysis of the complex revealed a M_2L_2 cage-like with a methanol molecule beside the cage. The coordination number of Pb^{II} is eight, (PbN_3O_5) with a stereo-chemically active electron lone pair and the coordination sphere is hemi-directed.

PbO nanoparticles (~30 nm) were obtained by its thermolysis at 180 °C with oleic acid as a surfactant, similar to the reported above reactions of 2,9-dimethyl-1,10-phenanthroline complexes. Crystalline and nano-structures of two Pb(II) coordination polymers, $[Pb_2(2\text{-pyr})_4(MeOH)]_n$ {2-Hpyr = 2-pyrazinecarboxylic acid, **15**} and $[Pb(2\text{-quc})_2]_n$ {2-Hquc = 2-quinolinecarboxylic acid, **16**}, were synthesized via thermal gradient and sonochemical methods, respectively [79]. The compounds were then heated to 600 °C to produce PbO nanoparticles. Interestingly, PbO nanoparticles with different morphology and size were produced by calcination of the two coordination polymers.

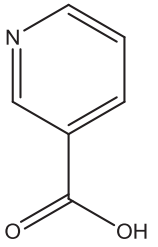

14

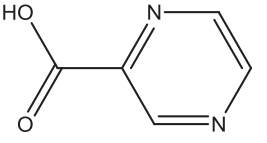

15

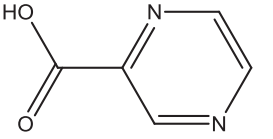

16

Mixed-oxide and other nanocomposites

A few mixed-oxide nanocomposites or binary oxides, produced from mixtures of metal complexes, are known. Mixed-metal oxalates were also used for preparation of bimetallic or mixed-oxide nanostructures. Thus, a family of 2-D polymetallic oxalate-bridged polymeric networks [80] with general formula $[M^{II}(H_2O)_2]_3[M^{III}(ox)_3]_2(18\text{-crown-}6)_2$ (M^{III}=Cr, Fe; M^{II}=Mn, Fe, Co, Ni; 18-crown-6), exhibiting ferro- (Cr^{3+}) or ferrimagnetic (Fe^{3+}) ordering in the 3.6–20 K interval depending on the nature of the trivalent metal ion, were used as precursors for generation of pure phases of mixed oxides with spinel-like structures as $(Mn,Co,Fe)_3O_4$, behaving as a magnet at r.t. Also, a facile one-pot procedure, or so-called "direct synthesis" [81], was used to prepare the heterometallic complexes $[M_2Mn(OAc)_6(bpy)_2]$, where M=Cu, Co, Zn, and bpy = 2,2′-bipyridine, with high yields via oxidative dissolution of pure metals in a liquid phase [82]. Corresponding metal oxide nanocomposites/binary oxides can be obtained by further heating of these compounds. Liquid-feed flame spray pyrolysis was also used to synthesize [83] Mg–Fe-based mixed-metal nanopowders in the $(MgO)_x(Fe_2O_3)_{1-x}$ system from metal-complex precursors. Iron propionate $[Fe(O_2CCH_2CH_3)_3]$ and magnesium acetylacetonate $[Mg(C_5H_7O_2)_2{\cdot}2H_2O]$ precursors were dissolved in ethanol, aerosolized with oxygen and combusted at 1500 °C and thereafter quenched rapidly. Final powders had a range of compositions (x = 0.30, 0.45, 0.50, 0.65, 0.75, and 0.90 ± 0.02) and particle sizes generally increased as the fraction of MgO increased. Finally, a cerium-triethanolamine complex was prepared and used as the precursor to synthesize well-crystallized CeO_2 nanoparticles (3~5 nm) [84, 85]. It was mixed with methylmethacrylate in aqueous solution and hydrolyzed to generate CeO_2 nanoparticles. The emulsion polymerization of the monomer was followed in one-pot, and a nano-CeO_2/poly(methylmethacrylate) composite was obtained. The thermal stability and glass-transmission temperature of the polymer were enhanced by incorporation of nano-CeO_2.

Sulfides, selenides, and phosphides

Complexes with S-containing ligands only, without any other heteroatoms (N, O, P, etc.), applied for nanostructure preparation, are practically unknown. In this respect, we note a review [86], where emerging role of complexes of dithiolate ligands **17**–**20** (i.e. dithiocarboxylates, xanthates, dithiocarbamates, dithiophosphates, dithiophophinates, and dithioarsenates) as single source molecular precursors for preparation of metal sulfide thin films and nano-particles is discussed. In case of indium, different phases of In_2S_3 can be generated either by changing the precursors or by subtle variation in pyrolytic conditions. *Tris*(xanthate) complexes of indium undergo a single-step decomposition leading to $In_2S_{3.71}$. Dithiocarbamate complexes undergo either a single step or two closely spaced step decompositions from 239 to 389 °C. Two pathways leading to formation of either indium metal (R = Et, Pr-*n*, Bu-*i*) or In_2S_3 (R = Me, Pr-*n*, Bu-*i*) were also identified. In case of nickel dithiocarbamates, highly regular urchin-like NiS architectures were synthesized on a large scale by solvothermal treatment of a single-source molecular precursor of nickel diethyldithiocarbamate [$Ni(DDTC)_2$] at 180 °C (reaction 11) [87]. These urchin-like architectures (figures 13 and 14), with an average diameter of 16 mm, were composed of single-crystalline NiS nanoneedles with a diameter of 100 nm and a length of up to 8 μm. It was revealed that the solvent medium can strongly affect the composition and crystal phases of the products, and a surfactant is crucial to form urchin-like patterns.

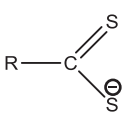

17

Dithiocarboxylates

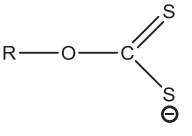

18

Xantates

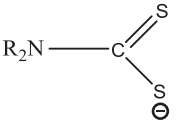

19

Dithiocarbamates

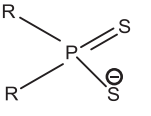

20

Dithiophosphates / phosphinates

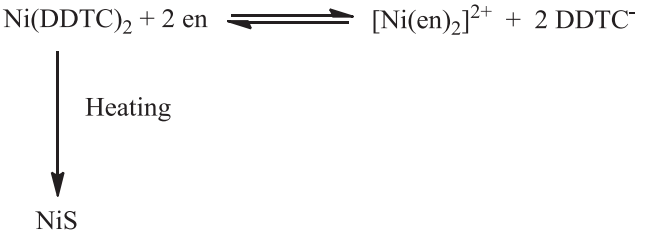

(11)

However, these metals above and below are incomparable with cadmium sulfide in respect of a variety of methods for preparation from metal complexes and formed nanostructures; this is due to its importance and a series of applications in nanotechnology. Thus, the *in situ* synthesis and patterning of CdS nanocrystals was carried out by laser processing of a transparent polymer matrix doped with a cadmium thiolate methylimidazole (MI) modified complex, $[Cd(SBz)_2]_2 \cdot MI$ [88]. The precursor structure ensures a uniform distribution inside the polymer and gives a regular and homogeneous network of CdS nanocrystals in

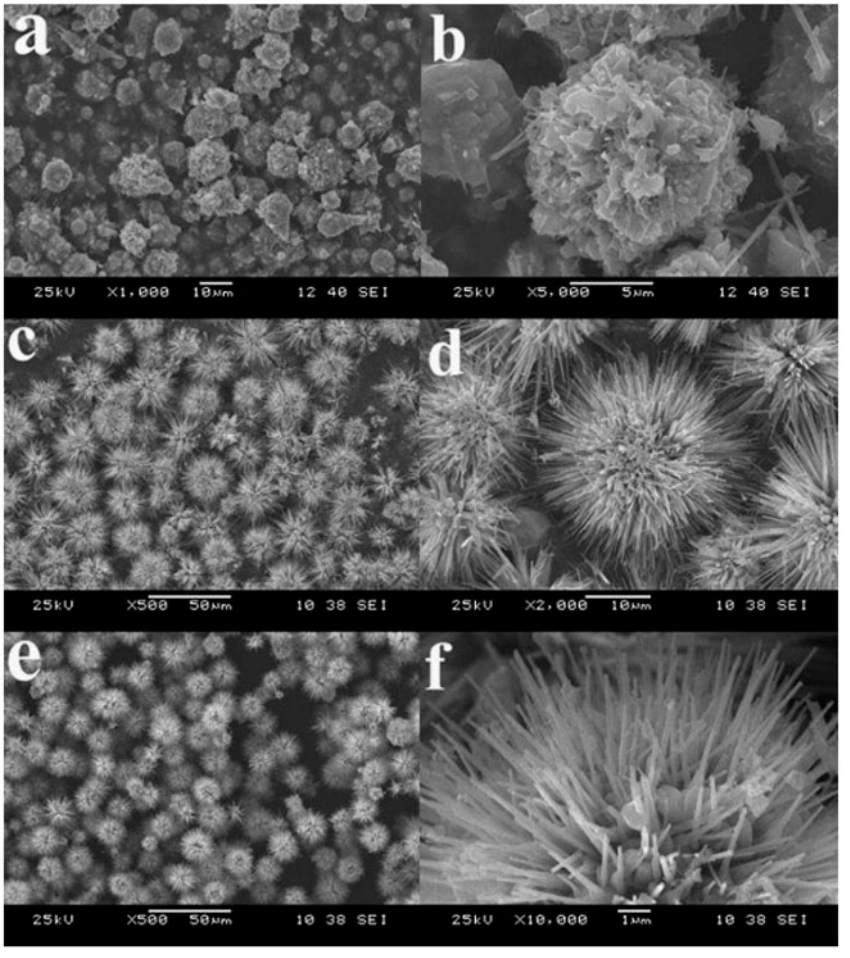

Figure 13. SEM images of the products synthesized in ethylenediamine with different surfactants: ((a) and (b)) without any surfactant; ((c) and (d)) CTAB; ((e) and (f)) PEG.

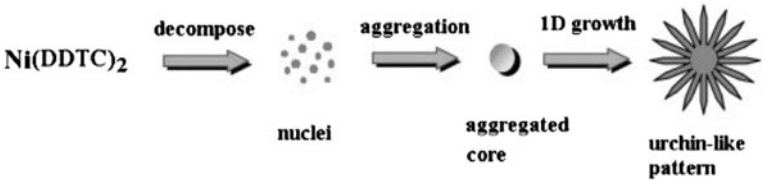

Figure 14. Schematic illustration of the possible formation process of the urchin-like NiS architecture.

the quantum size regime with a finely tunable bandgap by varying the laser fluence in the range 25–75 mJ cm^{-2} and shot number from 10 to 100. In a Cd(II) complex with bithiazole derivative, $[Cd(DADMBTZ)_2(NO_2)_2]$ (DADMBTZ = 2,2′-diamino-5,5′-dimethyl-4,4′-bithiazole **6**), the coordination number of cadmium is six with a distorted octahedral, CdN_4O_2 [89]. In reaction with DADMBTZ (mentioned also in the previous section), DADMBTZ is bidentate in complex to form five-membered chelate rings with different internal angles in the coordination polyhedron. The CdS nanoparticles were prepared using this complex as precursor via thermal decomposition. However, in thermal decomposition of $[Cd(DADMBTZ)_3](ClO_3)_2$ (prepared by reactions 12–14) an oxide-sulfide nanocomposite CdO–CdS was prepared [90].

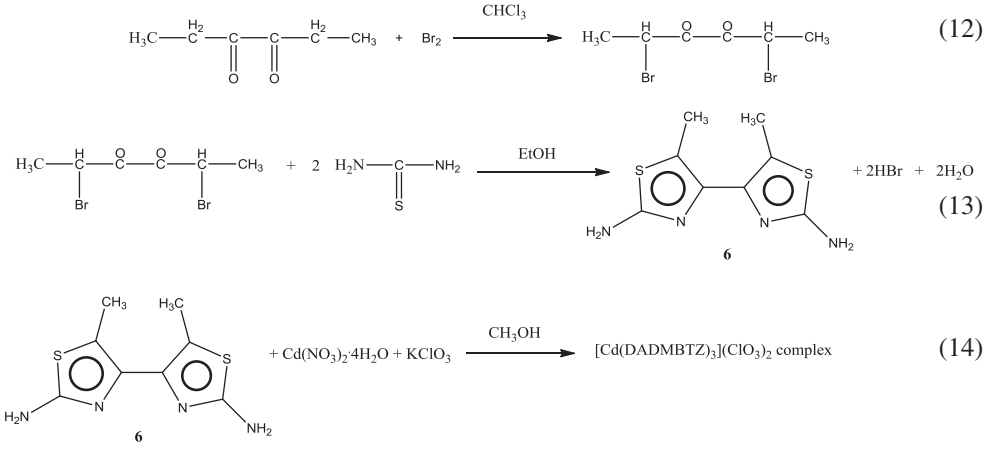

(12)

(13)

(14)

A convenient solvothermal single-source route was developed for the bulk synthesis of CdS nanorods using air stable dimeric cadmium(II) complex of S-benzyldithiocarbazate, $[Cd(PhCH_2SC(=S)NHNH_2)Cl_2]_2$, at a relatively low temperature (reaction 15) [91]. The decomposition of the precursor was made by heating at 160 °C in hexamethylenediamine (HMDA) to give amine capped CdS nanocrystals (rods) having yield ca. 90%. A template free fabrication of CdS microflowers was carried out by thermal decomposition of cadmium thiocyanate complex at 300 °C under open atmosphere [92]. This synthetic methodology opens a new window for a well crystallized, single phase CdS preparation in large-scale. The microflower morphology was self-assembled by intact thin nano-sheets. CdS nanoparticles with different shapes and sizes (rods and spheres, figure 15) were synthesized through decomposition of precursor complex (figure 16) $[Cd(SOCPh)_2Lut_2]$ {Lut = 3,5-dimethylpyridine (lutidine)} (P_21/n) using structure-directing solvents such as ethylenediamine, dimethylsulfoxide, and ammonia, as well as by thermal decomposition of the precursor complex under N_2 (reactions 16 and 17) [93]. The photo-catalytic activity of CdS nanoparticles was studied by the degradation of Rose Bengal dye, indicating an excellent photocatalytic activity compared to that of commercial TiO_2. Also, an intrinsic peroxidase-like activity of CdS nanoparticles was demonstrated toward peroxidase substrates 3,3′,5,5′-tetramethyl benzidine and hydrogen peroxide.

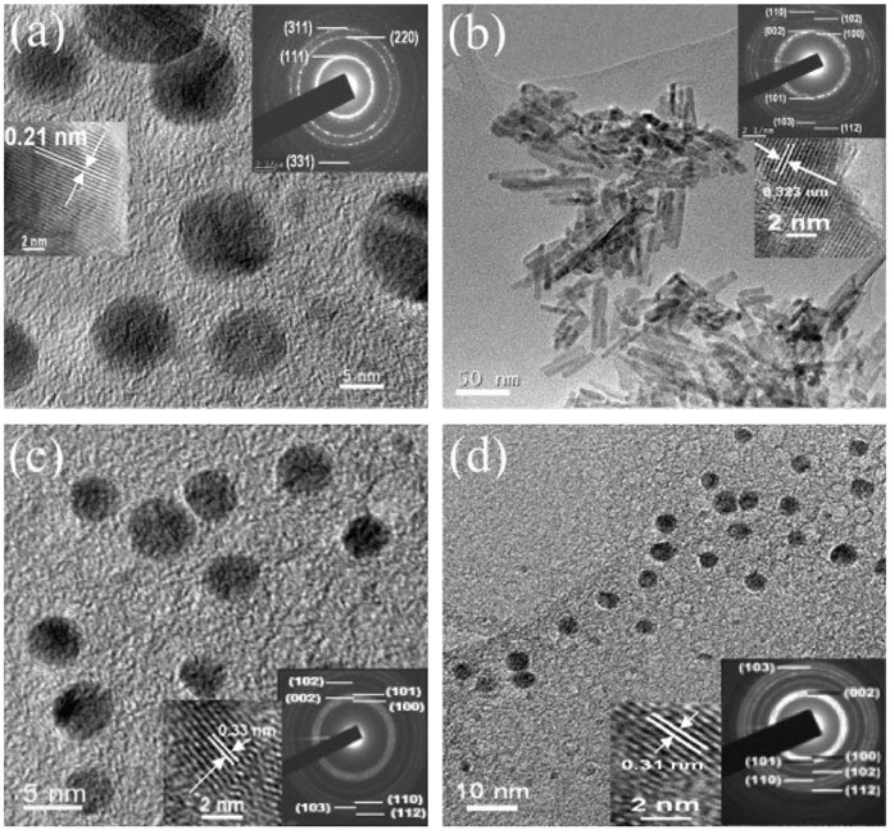

Figure 15. TEM images (inset: corresponding SAED pattern and lattice fringe) for CdS nanoparticles obtained from (a) HT (high temperature), (b) EN, (c) DMSO, and (d) NH_3.

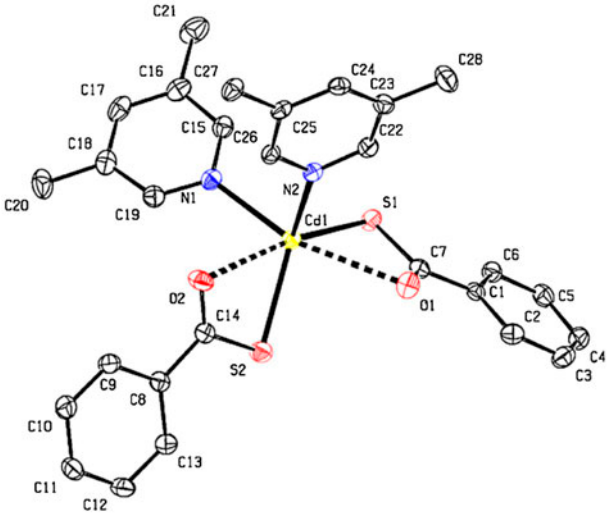

Figure 16. ORTEP diagram of the single-source precursor complex $[Cd(SOCPh)_2Lut_2]$.

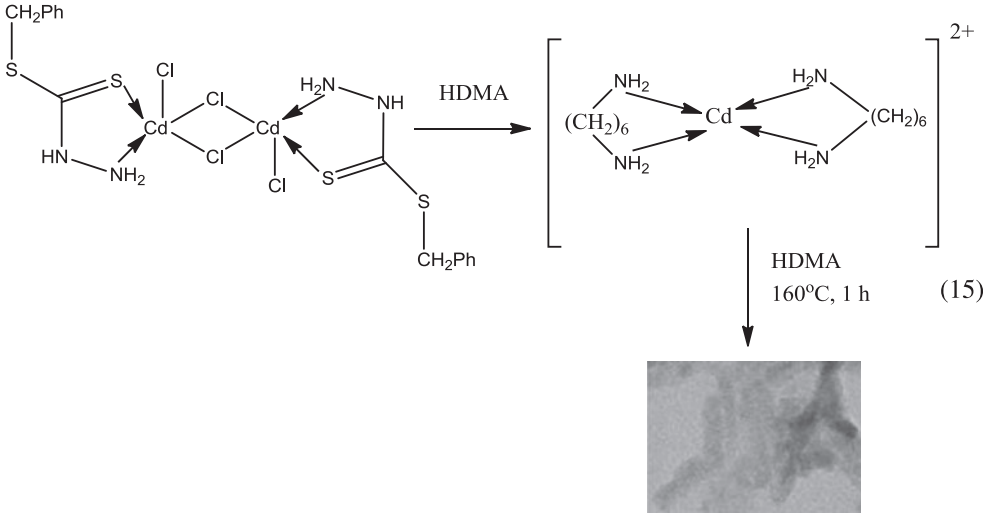

(15)

Formation of CdS nanorods by decomposition of $[Cd(PhCH_2SC(=S)NHNH_2)Cl_2]_2$.

$$Cd(SOCPh)_2 \cdot Lut_2 \rightarrow CdS\ Lut_2 + S(OCPh)_2 \quad (16)$$

$$CdS\ Lut_2 \rightarrow CdS + 2Lut \quad (17)$$

The reactions of 4-bromo-1-(2-chloroethyl)-1H-pyrazole prepared from 4-bromopyrazole with the *in situ* generated PhSNa, PhSeNa, Na_2S, and Na_2Se resulted [94] in thio/selenoether ligands L^1–L^4, respectively. The complexes $[PdL^1/L^2Cl_2]$ and $[PdL^3/L^4Cl]BF_4$ of these ligands were synthesized by reacting them with $[PdCl_2(CH_3CN)_2]$ in CH_3CN at 70 °C. Single source one-pot synthesis of Pd_4Se and PdSe nanoparticles (size ranges ~8–26 nm), capped with trioctylphosphine (TOP), was developed by thermolysis of the complexes with L^2 and L^4 at 200–250 °C in TOP. Nanoparticles of PdP_2 were formed when attempts were made to prepare nano-sized phases of palladium-sulfide by thermolysis of complexes with L^1 and L^3 in TOP. A template free and low-temperature hydrothermal reaction pathway using Cu(II) – thiourea complex (prepared *in situ* from copper(II) chloride and thiourea as precursors) and citric acid as complexing agent to synthesize 2-D hierarchical nano-structures (figure 17) of covellite CuS (also known as covelline) was reported [95]. With heating under hydrothermal condition, thiourea decomposes to generate hydrogen sulfide (H_2S); the produced H_2S reacts with solution Cu^{2+} producing CuS (reactions 18 and 19). Alternatively, pure nanocrystalline form (21–34 nm size) of the same covellite phase CuS was similarly synthesized [96] by reaction of copper acetate and thiourea with addition of sodium hydroxide, by chemical precipitation at 30 °C. The particle size and yield depended on reaction time, amount of reactants, temperature, and also on the amount of reducing agent used.

$$NH_2CSNH_2 + 2H_2O \rightarrow 2NH_3 + H_2S + CO_2 \quad (18)$$

$$CuCl_2 + H_2S \rightarrow CuS + 2HCl \quad (19)$$

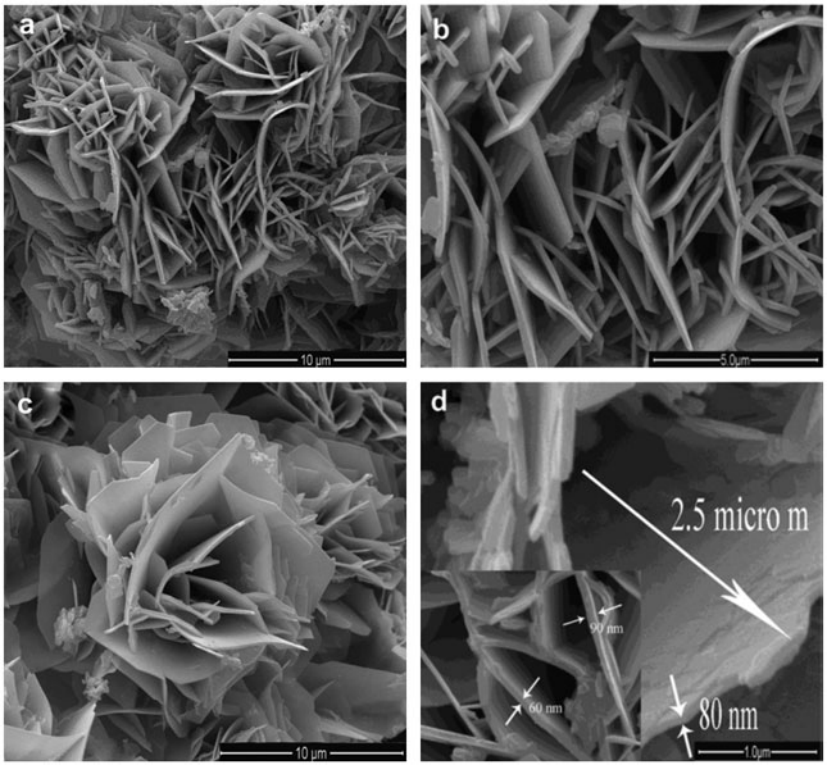

Figure 17. Microstructure of as prepared CuS powder in the presence of 0.2 M citric acid solution in the hydrothermal precursor, in order of increasing magnification from ((a) and (b)). (c) Shows a rose-like micro-architecture formed (d) and its inset are high magnification views of specified portions to reveal the thickness and lengths of nano-sheets.

Nanostructured PbSe materials were prepared via a solvothermal method at 180 °C using lead precursors containing Schiff bases {Pb(salpn) and Pb(salophen)}, $SeCl_4$ and $N_2H_4 \cdot H_2O$ as starting materials and propylene glycol as solvent [97]. The ligands were synthesized from 1,3-propylenediamine or 2-phenylenediamine with salicylaldehyde in ethanol. PbSe nanostructures with lower particle size were obtained after solvothermal treatment for 3 h at 180 °C in the presence of hydrazine hydrate as reducing agent. Pure cubic phase PbSe nanostructures with homogeneous particle size could be prepared by Pb (salpn) as precursor through a solvothermal method at 180 °C. Additionally to the cubic structures, particle-like PbSe nanoforms were also observed. According to the authors, the solvothermal formation mechanism of PbSe nanostructures is probably related to the dissociation of lead precursor under high temperature and pressure to release Pb^{2+}. Then, the Se^{2-} ions produced by reaction between $SeCl_4$ and hydrazine hydrate react with the Pb^{2+} to form PbSe nuclei (hydrazine hydrate can reduce $SeCl_4$ to bivalent anion). The growth of PbSe nuclei occurs during the thermal treatment process, and PbSe nanostructures are produced (reactions 20–22). Similarly to the lead selenide above, nanoscale metal sulfides can be obtained from non-S-containing complexes and sulfur source. Thus, micro/nanoscale spherical HgS was isolated by reaction of $Na_2[Hg(HL)_2(H_2O)_2]$ {1 : 2 (M : L)

chelate complex} with alkaline solution of thiourea in aqueous solution phase [98]. The metal chelate complex was prepared by reaction of Hg(II) with 2-hydroxy-1-(1-hydroxy-2-naphthylazo)-6-nitronaphthalene-4-sulphonic acid sodium salt; eriochrome black T (EBT, NaH_2L) in alkaline medium. Finally, nanostructures of metal chalcogenides (if Se was present in the ligand together with phosphorus) and more complex products consisting of capped/core-shell structures can be obtained from metal complexes of P-containing ligands. Thus, $CuInSe_2$, $CuGaSe_2$, and $CuIn_{(1-x)}Ga_xSe_2$ nanoparticles (3–14 nm) were synthesized from diisopropyldiselenophosphinatometal complexes $M_x[i\text{-}Pr_2PSe_2]_n$ {M=Cu(I), In(III), Ga(III); n = 1, 3} by thermal decomposition of the precursors in HDA/TOP at 120–210 °C or 250 °C [99].

$$\text{Lead Schiff base} \rightarrow Pb^{2+} + \text{other pyrolysis products} \tag{20}$$

$$2SeCl_4 + 3N_2H_4 \cdot H_2O\ (N_2H_5^+) \rightarrow 2Se^{2-} + 3N_2 + 15H^+ + 8Cl^- \tag{21}$$

$$Pb^{2+} + Se^{2-} \rightarrow PbSe \tag{22}$$

An interesting example of growth of metal phosphide (among others) nanostructures from organometallics is known for gallium. Thus, the growth and characterization of 3-D structures (Ga_2O_3, $CuGa_xO_y$ and (Ga, In)P nanowires) using organometallic precursors like M $(CH_3)_3$ (M is Cu, Ga, and In) was discussed [100]. These structures can be separated into two classes: (a) one with (Ga, Al, In) metallic alloys shaped as sphere, scepter, or cylinder and a carbon membrane covering the alloy; (b) the other with semiconductor or oxide nanowires capped by a metallic sphere. The growth of such gallium nanostructures is presented in figure 18; it is performed by exposition and interaction of organometallic vapor with a substrate within a MOCVD apparatus (reactions 23 and 24). At low temperature, 450–550 °C, the growth of thin leaf-like structures, called by authors as 3-D grass structures, were observed. At relatively higher temperature, 600–750 °C, structures such as balloons and cylinders were obtained. By using an intermediate temperature, 550–600 °C, and low carrier (N_2) gas flow, neurone-like structures were synthesized. Growth products $CuGa_xO_y$ (wire) and (Ga, In)P (bamboo) are shown in figures 19 and 20, respectively.

$$\begin{aligned}&\text{TMGa (trimethylgallium)} + \text{InP } 650\,^\circ\text{C}\\ &\quad\rightarrow \text{GaInP wire capped by (Ga, In) ball} + \text{carbon radicals}\end{aligned} \tag{23}$$

$$\text{TMGa} + \text{TMIn} + \text{InP } 650\,^\circ\text{C} \rightarrow \text{GaP wire capped by (Ga) ball} + \text{carbon radicals} \tag{24}$$

Ferrites, titanates, and zirconates

A series of recent reports are devoted to ferrites of various transition metals. The influence of aging time of the iron–cobalt oleate precursor on the structure, chemical composition, size, and magnetic relaxation of cobalt ferrite nanoparticles synthesized by thermal decomposition was studied [101]. The resulting nanoparticles would be suitable for sensors based on the Brownian relaxation mechanism and in determining mechanical properties of

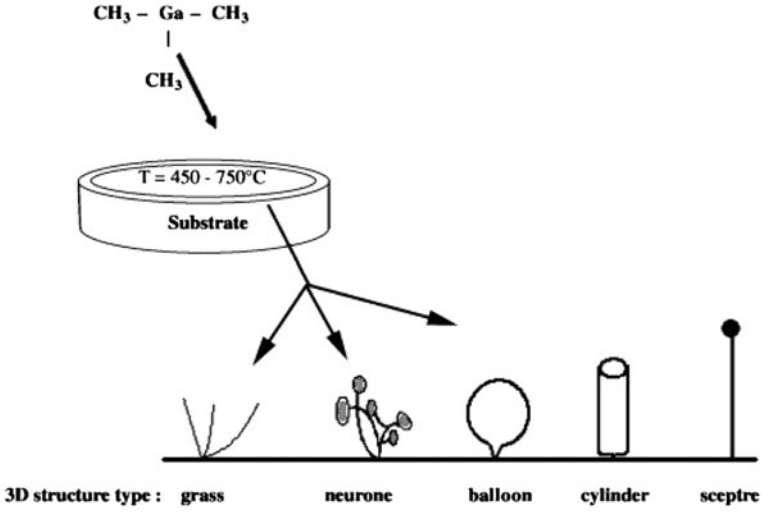

Figure 18. Picture representing 3-D structures grown by exposure of a substrate to a TMGa organometallic precursor flow (~1 sccm). Carrier gas flow: N_2: 2–10 slm. Its growth depends on the reactor conditions (50–760 Torr), giving rise to grass leaf (450–550 °C), neurone (550–600 °C), balloon, cylinder, and scepter (600–750 °C) shaped structures. Most of these structures are held by carbon membranes and contain Ga inside. Growth duration is 5–15 min.

complex fluids at the size scale of the nanoparticles. Thermal decomposition of the trinuclear heterometallic oxo, acetates $[Fe_2M(\mu_3\text{-}O)(CH_3COO)_6(H_2O)_3]$ was used as a single-precursor method for synthesis of the spinel-structured highly pure stoichiometric ternary oxides (7–20 nm in size) MFe_2O_4 ($M=Mn^{II}$, Co^{II}, and Ni^{II}) at 320 °C. Their magnetic properties from 10–300 K revealed superparamagnetic behavior for the Ni and Mn particles and ferrimagnetic behavior for the Co ones at r.t. [102]. Nickel and iron alkoxide complex, $NiFe_2(OCH_2CH_2OH)_8$, was directly synthesized [103] by electrolysis of nickel and iron in $HOCH_2CH_2OH$ solution. The nickel ferrite $NiFe_2O_4$ nanopowder of 25–40 nm was obtained in high purity by a direct sol–gel of the above solution following taking to dryness at 400 °C for 2 h. Alternatively, an economical method, the modified powder process, was developed for synthesis of $NiFe_2O_4$ at temperatures as low as 850 °C [104]. The method is based on pyrolysis of a precursor consisting of a fine iron oxide powder combined with $Ni(L)_2$ (L = acetate, acetylacetonate, gluconate). Upon heating, the decomposition of $Ni(L)_2$ leads to coating of the iron oxide particles with nickel oxide, yielding a precursor powder in which the two component oxides are more homogeneously mixed than that which can be achieved by simple mixing of the metal oxides according to conventional powder processing. For α and γ iron(III) oxide powders of similar particle size, ferrite nucleation was found to occur at lower temperature (875 °C) for the precursor $Ni(acetate)_2\text{-}\gamma\text{-}Fe_2O_3$ while 1000 °C was required to generate pure ferrite from $Ni(acetate)_2\text{-}\alpha\text{-}Fe_2O_3$. The morphologies and surface area of the products were found to depend strongly on the nickel oxide precursor; high surface area porous solids were obtained when using nickel acetate, large-grained $NiFe_2O_4$ was produced when using nickel acetylacetonate, while the nickel gluconate yielded a tortuous web-like material with large pores.

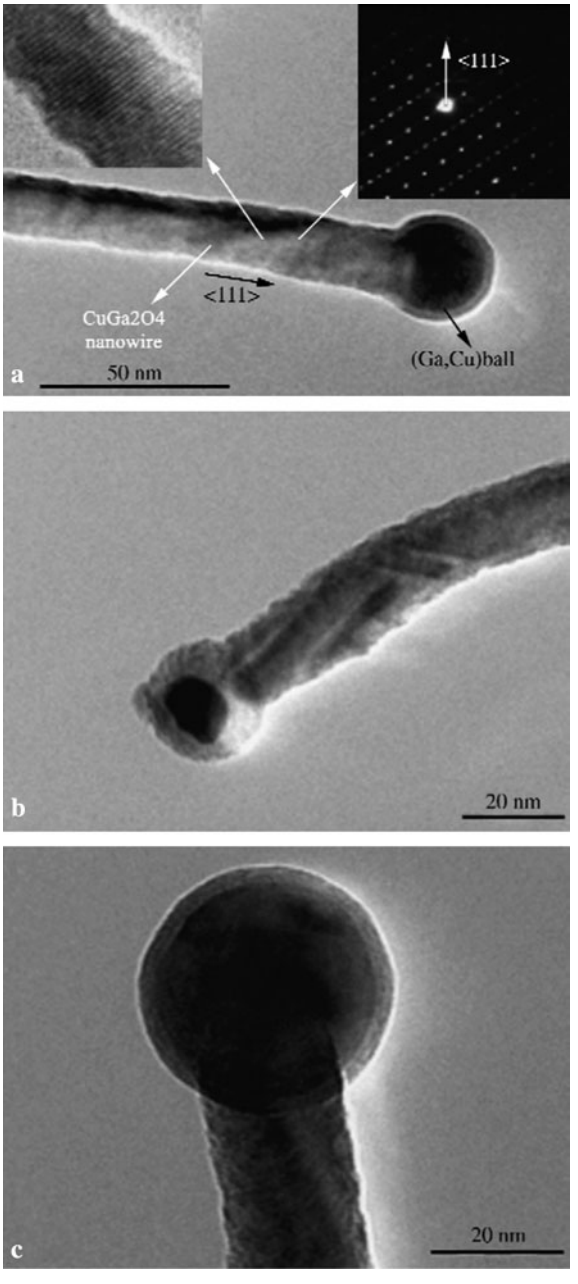

Figure 19. (a) High-resolution TEM bright field picture, and selected area electron diffraction pattern inset of a $CuGa_2O_4$ wire grown on Cu at 650 °C during 15 min; (b) and (c) HRTEM bright field image of $CuGa_2O_4$ nanowire single crystals. Note that the interface between wire/ball and top of the ball can be (a) flat/round; (b) round/flat; and (c) round/round.

Hydrazine N_2H_4, a common solvent and weak reductant, was utilized as ligand in a manganese zinc ferrous fumarato(**21**)-hydrazinate precursor, $Mn_{0.6}Zn_{0.4}Fe_2(C_4H_2O_4)_3 \cdot 6N_2H_4$ [105]. This compound on touching with burning splinter underwent self-propagating

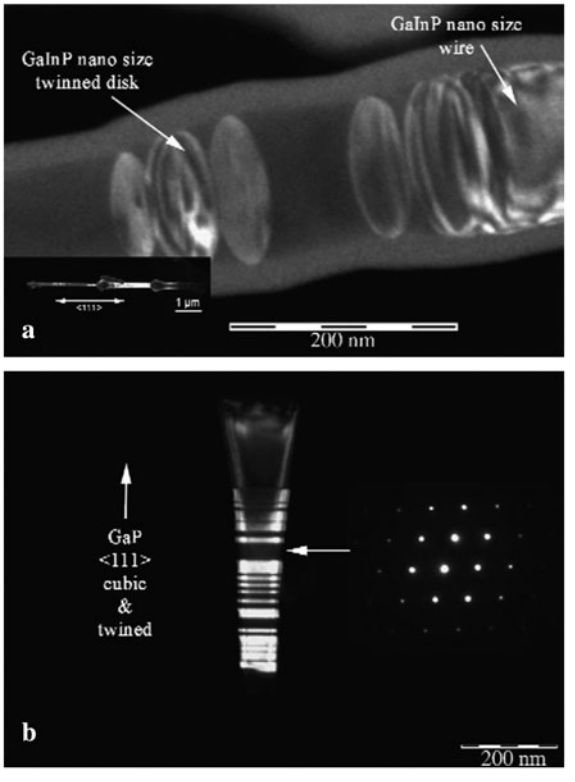

Figure 20. (a) HRTEM pictures of a bamboo shaped GaInP from InP exposed to TMGa flow (SEM inset on the left) and (b) HRTEM picture of a GaP wire made of twined single crystal nanostructure from InP exposed to TMGa and TMIn flow. Both structures are grown on InP by MOCVD at 650 °C during 15 min.

autocatalytic decomposition yielding ultra-fine $Mn_{0.6}Zn_{0.4}Fe_2O_4$. The saturation magnetization of the as-prepared $Mn_{0.6}Zn_{0.4}Fe_2O_4$ was 31.46 emu/g. Mn–Ni–Zn ferrite nanoparticles (10 nm) were similarly prepared [106], as well as $Ni_{0.6}Zn_{0.4}Fe_2O_4$ (20 nm) [107]. Several alkoxide complexes, related to Ni $Fe_2(OCH_2CH_2OH)_8$, were also applied for titania-based nanostructures. In a cell without separating the cathode and anode spaces, Ni and Ti alkoxide complex was synthesized [108] by electrochemical dissolution of Ti for 6 h, and of Ni for 3 h at 40 °C in $CH_3OCH_2CH_2OH$ solution of $(Bu_4N)Br$. It was shown that the precursor of $NiTiO_3$ is $NiTi(OCH_2CH_2OCH_3)_6$. The xerogel was obtained by bringing to dryness in vacuum for 24 h and hydrolysis under pH 9 of the precursor, which was heated at 520 °C for 2 h to obtain the $NiTiO_3$ nano powder. Also, the hydrothermal method was applied to obtain a mixed-metal metal-organic framework compound $[NiMn_2\{C_6H_3(COO)_3\}_2]$ by replacing one of the octahedral Mn^{2+} ions in $[Mn_3\{C_6H_3(COO)_3\}_2]$ by Ni^{2+} [109]. On heating in flowing air, it transformed to nanosized ferromagnetic $NiMn_2O_4$ spinel at low temperature (400 °C). The transition temperature of $NiMn_2O_4$ nanoparticles exhibited a direct correlation with the particle size.

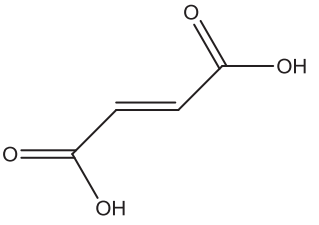

21 fumaric acid

Perovskite-structured lead titanate thin films were grown on FTO-coated glass substrates from a single-source heterometallic molecular complex, $[PbTi(\mu_2\text{-}O_2CCF_3)_4(THF)_3(\mu_3\text{-}O)]_2$ (figure 21), which was isolated in quantitative yield from reaction of tetraacetatolead(IV), tetrabutoxytitanium(IV), and trifluoroacetic acid from a tetrahydrofuran solution [110]. Thin films of lead titanate having spherical particles of various sizes were grown by aerosol-assisted CVD at 550 °C. An optical band gap of 3.69 eV was estimated by UV–visible spectrophotometry. According to the authors, this complex is unique in the sense that it contains all of the necessary components of $PbTiO_3$ bonded in one structure and thermally decomposes at 550 °C under mild AACVD conditions to yield thin films (figure 22) of crystalline $PbTiO_3$ having a band gap of 3.69 eV that may be used for various technological and photocatalytic applications. Lastly, the synthesis of $Ce_xZr_{1-x}O_2$ and $(Ce_{0.7}Zr_{0.3}O_2)_x(Al_2O_3)_{1-x}$ core-shell nanopowders (about 20 nm of particle size and specific surface areas of 30–50 m^2/g) were obtained in a single step [111] by liquid-feed flame spray pyrolysis (LF-FSP) of the precursors $Ce(O_2CCH_2CH_3)_3(OH)$, alumatrane $[N(CH_2CH_2O)_3Al]$, and $Zr(O_2CCH_2CH_3)_2(OH)_2$. Solutions of all three precursors in ethanol with ceramic yields of 2.5 wt.% were aerosolized with O_2, combusted at temperatures above 1500 °C, and rapidly quenched at ~1000 °C/ms to form nanopowder products of selected compositions at rates of

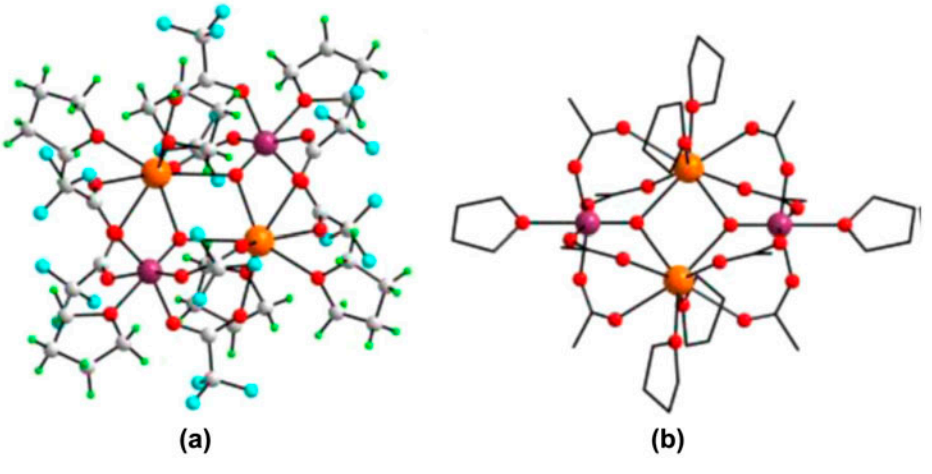

Figure 21. Two views of the molecular structure of $[PbTi(\mu_2\text{-}O_2CCF_3)_4(THF)_3(\mu_3\text{-}O)]_2$: (a) full molecule drawn with arbitrary ellipsoids; (b) molecule without F and H atoms (the organic residues are shown in stick form). The disordered components have been omitted for clarity. Color code: Pb, orange; Ti, violet; F, cyan; O, red; C, gray; H, green (see http://dx.doi.org/10.1080/00958972.2013.851382 for color version).

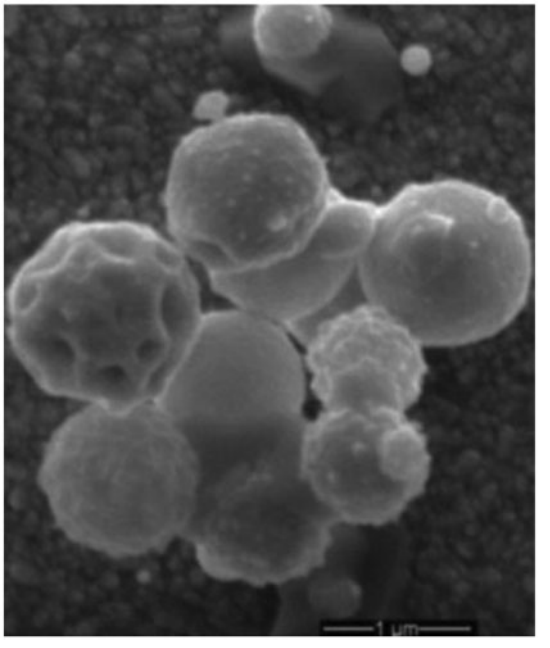

Figure 22. SEM image of a thin film of $PbTiO_3$ showing transparent spherical particles with a glassy appearance.

50–100 g/h. These materials offer significant catalytic activities for hydrocarbon oxidation processes without using platinum as a co-catalyst.

Conclusions

Coordination and organometallic compounds are suitable to use for inorganic nanoparticle formation due to their relatively low stability and availability to be reduced to metals or thermodynamically stable oxides. Complexes of N–, O–, N, O–, N, S(Se)–, O, S(Se)–, N, O, S(Se)–, and N, P-containing ligands as well as σ- and π-organometallic compounds have been used as precursors, even classic N-containing Werner ligands. The range of temperatures for destruction of metal complexes is wide (100–700 °C), depending on their stability. For example, acetylacetonates decompose usually at 100–150 °C forming oxide nanofilms. On the basis of the revised bibliography, it can be observed that complexes of some types of ligands are generally used as precursors for certain metals. Thus, for example, coordination compounds with N-containing ligand systems are applied for formation of mainly lead (II) oxide nanoparticles; complexes of sulfur-containing ligands are used for cadmium sulfide nanoparticles, one of most important objects in nanotechnology.

Among a variety of applied methods, pyrolysis and CVD techniques are common. Laser processing is also widely applied, in particular for creation of a transparent polymer matrix doped with complexes. Ultrasonic treatment of complexes sometimes is the only way to get nanoparticles without their further agglomeration. It should be emphasized that MOCVD, plasma-assisted CVD, combustion, laser, electron beam irradiation, and related sophisticated techniques are mainly utilized with organometallics as precursors.

Various classic and less-common nano- and microstructures [112] can be obtained by the methods above, in particular intermetallic nanoparticles, spherical nanoparticles, microflowers, nanourchins, nanofilms, nanorods, nanoleaves, nanoballoons, nanoneurones, and nanowires, bamboo-like and cylinder-like, especially from S-containing complexes. The shape of nanoparticles can be controlled using structure-directing solvents such as ethylenediamine, dimethylsulfoxide, and ammonia. The formed nanoparticles are frequently of an ultra-small size (<10 nm). Nanoparticles can be obtained in supported form (inside the cavities as Pd nanoparticles in MOF-5) or be doped (Mn/ZnO).

In case of metals, starting from coordination compounds and organometallics, nanosized metals (1) have been fabricated in free and supported forms, (2) are mainly transition and noble metals and (3) can form bimetallic nanoparticles. For transition metals, we note that mainly bimetallic compounds or more complex composites have been obtained from a variety of metal complexes containing the simplest and more sophisticated ligands.

Metal complexes can be used for preparation of nanoparticles, containing elements which were not part in these complexes. For example, sulfide nanoparticles can be produced by non–pyrolytic reactions of non-S-containing complexes and sulfur source. In addition, $(NH_4)_{18}[(Mo_2O_4)_6(OH)_6(O_3PCH_2PO_3)_6]\cdot 33H_2O$ and $Na_8[(Mo_2O_4)_3(O_3PCH_2PO_3)_3(CH_3AsO_3)]\cdot 19H_2O$ were found to be very efficient both as reductants of Pt and Pd metallic salts and as capping agents for the resulting Pt^0 and Pd^0 nanoparticles.

Taking into account an increased number of reports in the reviewed field during the past five years, we conclude that the use of metal complexes in fabrication of classic and rare nanostructures could be converted into a hot topic in the frontiers of coordination/organometallic chemistry and nanotechnology.

References

[1] S. Yang, R.E. Bachman, X. Feng, K. Mullen. *Acc. Chem. Res.*, **46**, 116 (2013).
[2] G. Kedarnath, V.K. Jain. Pyridyl and pyrimidyl chalcogen (Se and Te) compounds: A family of multi utility molecules. *Coord. Chem. Rev.*, **257**, 1409 (2013).
[3] M. Zhang, J. Guan, B. Zhang, D. Su, C.T. Williams, C. Liang. *Catal. Lett.*, **142**, 313 (2012).
[4] Z.L. Hu, M. Aizawa, Z.-M. Wang, N. Yoshizawa, H. Hatori. *Langmuir*, **26**, 6681 (2010).
[5] A. Dolbecq, J.-D. Compain, P. Mialane, J. Marrot, F. Sécheresse, B. Keita, L.R.B. Holzle, F. Miserque, L. Nadjo. *Chem. Eur. J.*, **15**, 733 (2009).
[6] S.S. Zalesskiy, V.P. Ananikov. *Organometallics*, **31**, 2302 (2012).
[7] J.L. Rouge, C.J. Ackerson, D.L. Feldheim, B.E. Eaton. *J. Mater. Chem.*, **20**, 8394 (2010).
[8] E. Ramírez-Meneses, V. Montiel-Palma, V.H. Chávez-Herrera, J. Reyes-Gasga. *J. Mater. Sci.*, **46**, 3597 (2011).
[9] A.V. Zadesenets, T.I. Asanova, E.S. Vikulova, E.Y. Filatov, P.E. Plyusnin, I.A. Baidina, I.P. Asanov, S.V. Korenev. *J. Solid State Chem.*, **199**, 71 (2013).
[10] J.D. Wnuk, J.M. Gorham, S.G. Rosenberg, W.F. van Dorp, T.E. Madey, C.W. Hagen, D.H. Fairbrother. *J. Phys. Chem. C*, **113**, 2487 (2009).
[11] N.S. Hosmane, Z. Yinghuai, J.A. Maguire, W. Kaim, M. Takagaki. *J. Organomet. Chem.*, **694**, 1690 (2009).
[12] M. Tristany, K. Philippot, Y. Guari, V. Collière, P. Lecante, B. Chaudret. *J. Mater. Chem.*, **20**, 9523 (2010).
[13] S.B. Gadri, T.M. Keller, M. Laskovski, C.A. Little, P. Lubitz, M.S. Osofsky, H.R. Khan. *Appl. Phys. A*, **86**, 391 (2007).
[14] B. El Hamaoui, L. Zhi, J. Wu, J. Li, N.T. Lucas, Z. Tomović, U. Kolb, K. Müllen. *Adv. Funct. Mater.*, **17**, 1179 (2007).
[15] J.D. Wnuk, M. Gorham, S.G. Rosenberg, W.F. van Dorp, T.E. Madey, C.W. Hagen, D.H. Fairbrother. *J. Appl. Phys.*, **107**, 054301 (2010).
[16] M. Hashempour, H.R. Rezaie, H. Razavizadeh, M.T. Salehi, H. Mehrjoo, H. Ardestani. *J. Nano Res.*, **11**, 57 (2010).
[17] C. Díaz, M.L. Valenzuela. *J. Inorg. Organomet. Polym. Mater.*, **16**, 419 (2006).
[18] A. Meffre, S. Lachaize, C. Gatel, M. Respaud, B. Chaudret. *J. Mater. Chem.*, **21**, 13464 (2011).

[19] N. Atamena, D. Ciuculescu, G. Alcaraz, A. Smekhova, F. Wilhelm, A. Rogalev, B. Chaudret, P. Lecante, R.E. Benfieldd, C. Amiens. *Chem. Commun.*, **46**, 2453 (2010).
[20] Y. Chen, X. Luo, G.-H. Yue, X. Luo, D.-L. Peng. *Mater. Chem. Phys.*, **113**, 412 (2009).
[21] K. Lee, S.W. Kang, S.-U. Lee, K.-H. Park, Y.W. Lee, S.W. Han. *ACS Appl. Mater. Interfaces*, **4**, 4208 (2012).
[22] S. Arockiasamya, T. Maiyalagan, P. Kuppusami, C. Mallika, K.S. Nagaraja. *Micro Nanosystems*, **4**, 199 (2012).
[23] G. Suresh, P. Saravanan, D. Rajan Babu. *J. Magn. Magn. Mater.*, **324**, 2158 (2012).
[24] R. Alexandrescu, I. Morjan, F. Dumitrache, R. Birjega, C. Fleaca, I. Morjan, M. Scarisoreanu, C.R. Luculescu, E. Dutu, V. Kuncser, G. Filoti, E. Vasile, V. Ciupina. *Appl. Surf. Sci.*, **258**, 9421 (2012).
[25] T.K. Barkley, J.E. Vastano, J.R. Applegate, S.D. Bakrania. *Adv. Mater. Sci. Eng.*, **8** (2012).
[26] B.S. Lim, A. Rahtu, J.-S. Park, R.G. Gordon. *Inorg. Chem.*, **42**, 7951 (2003).
[27] Z. Li, S.T. Barry, R.G. Gordon. *Inorg. Chem.*, **44**, 1728 (2005).
[28] H. Li, T. Aaltonen, Z. Li, B.S. Lim, R.G. Gordon. *Open Inorg. Chem. J.*, **2**, 11 (2008).
[29] P.A. Lin, R.M. Sankaran. *Angew. Chem. Int. Ed.*, **50**, 10953 (2011).
[30] O.V. Kharissova, B.I. Kharisov, T. Hernández García, U. Ortiz Méndez. *Synth. React. Inorg. Met.-Org. Nano-Met. Chem.*, **39**, 662 (2009).
[31] J.J. Schneider, R.C. Hoffmann, J. Engstler, A. Klyszcz, E. Erdem, P. Jakes, R.-A. Eichel, L. Pitta-Bauermann, J. Bill. *Chem. Mater.*, **22**, 2203 (2010).
[32] E. Conterosito, G. Croce, L. Palin, E. Boccaleri, W. Van Beek, M. Milanesio. *CrystEngComm.*, **14**, 4472 (2012).
[33] A.A. Bagabas, A.W. Apblett, A.M. Shemsi, Z.S. Seddigi. *Main Group Chem.*, **7**, 65 (2008).
[34] K. Akhbari, A. Morsali. *J. Coord. Chem.*, **64**, 3521 (2011).
[35] A. Mehrani, A. Morsali, P. Ebrahimpour. *J. Coord. Chem.*, **66**, 856 (2013).
[36] M.H. Habibi, E. Askari. *Synth. React. Inorg. Met.-Org. Nano-Met. Chem.*, **43**, 406 (2013).
[37] A. Hosseinian, S. Jabbari, A. Reza Mahjoub, M. Movahedi. *J. Coord. Chem.*, **65**, 2623 (2012).
[38] A. Hosseinian, S. Jabbari, H.R. Rahimipour, A.R. Mahjoub. *J. Mol. Struct.*, **1028**, 215 (2012).
[39] M. Ranjbar, N. Shahsavan, M. Yousefi. *Am. Chem. Sci. J.*, **2**, 111 (2012).
[40] V. Safarifard, A. Morsali. *Ultrason. Sonochem.*, **19**, 1227 (2012).
[41] Y. Hanifehpour, B. Mirtamizdoust, S.W. Joo. *Z. Anorg. Allg. Chem.*, **638**, 357 (2012).
[42] M. Zheng, H. Zhang, X. Gong, R. Xu, Y. Xiao, H. Dong, X. Liu, Y. Liu. *Nanoscale Res. Lett.*, **8**, 166 (2013).
[43] Y. Ponco Prananto, M. Misbah Khunur, D. Tri Wahyuni, R. Arief Shobirin, Y. Rizky Nata, E. Riskah. *Bull. Chem. React. Eng. Catal.*, **7**, 198 (2013).
[44] J.Y. Park, S.-W. Choi, S.-H. Jung, S.S. Kim. *J. Nanosci. Nanotechnol.*, **12**, 1288 (2012).
[45] L.A. Saghatforoush, R. Mehdizadeh, F. Chalabian. *Transition Met. Chem.*, **35**, 903 (2010).
[46] A. Tahmasian, A. Morsali. *Inorg. Chim. Acta*, **387**, 327 (2012).
[47] A. Mehrani, A. Morsali. *J. Inorg. Organomet. Polym. Mater.*, **21**, 476 (2011).
[48] A. Brandt, A. Balducci. *J. Power Sources*, **230**, 44 (2013).
[49] O.V. Kharissova, J.R. Cardenas. *Phys. Status Solidi C: Conf. Crit. Rev.*, **2**, 3063 (2005).
[50] O.V. Kharissova. *Rev. Adv. Mater. Sci.*, **7**, 50 (2004).
[51] H.L. Wan, W. Deligeer, S. Zhao, S. Asuha. *Adv. Mater. Res.*, **624**, 55 (2013).
[52] B.I. Kharisov, R. Dias, V.M. Jimenez-Perez, O.V. Kharissova, B. Olvera Perez, B. Muñoz Flores. *RSC Adv.*, **2**, 9325 (2012).
[53] O.V. Kharissova, M. Garza Castañón, J.L. Hernández Pinero, U. Ortiz Méndez, B.I. Kharisov. *Mech. Adv. Mater. Struct.*, **16**, 63 (2009).
[54] J. Long, J. Dong, X. Wang, Z. Ding, Z. Zhang, L. Wu, Z. Li, X. Fu. *J. Colloid Interface Sci.*, **333**, 791 (2009).
[55] R. Gupta, S. Sanotra, H. Nawaz Sheikh, B. Lal Kalsotra, V. Kumar Gupta, Rajnikant. *J. Coord. Chem.*, **65**, 3917 (2012).
[56] L. Chen, C. Zhao, Z. Wei, S. Wang, Y. Gu. *Mater. Lett.*, **65**, 446 (2011).
[57] Y. Mu, J. Yang, S. Han, H. Hou, Y. Fan. *Mater. Lett.*, **64**, 1287 (2010).
[58] T. Waechtler, S. Oswald, N. Roth, A. Jakob, H. Lang, R. Ecke, S.E. Schulz, T. Gessner, A. Moskvinova, S. Schulze, M. Hietschold. *J. Electrochem. Soc.*, **156**, H453 (2009).
[59] A.D. Khalaji, D. Das. *J. Therm. Anal. Calorim.*, **114,** 671 (2013).
[60] M.S. Refat, M.Y. El-Sayed, A.M. Adam. *J. Mol. Struct.*, **1038**, 62 (2013).
[61] G.P. Nagabhushana, S. Ashoka, P. Chithaiah, G.T. Chandrappa. *Mater. Lett.*, **91**, 272 (2013).
[62] G.M. Neelgund, S.A. Shivashankar, B.K. Chethana, P.P. Sahoo, K.J. Rao. *Bull. Mater. Sci.*, **34**, 1163 (2011).
[63] V. Dhayal, M.K. Atal, B.L. Choudhary, M. Nagar, R. Bohra. *J. Sol-Gel Sci. Technol.*, **52**, 97 (2009).
[64] D. Ávila-Brande, R. Perezzan, E. Urones-Garrote, L.C. Otero-Díaz. *Inorg. Chem.*, **50**, 4640 (2011).
[65] A. Sartori, N. El Habra, C. De Zorzi, S. Sitran, M. Casarin, G. Cavinato, C. Sada, R. Gerbasi, G. Rossetto. *Chem. Vap. Deposition*, **18**, 151 (2012).
[66] J. Chandradass, K.H. Kim. *Mater. Manuf. Processes*, **24**, 541 (2009).

[67] A. Mahapatra, B.G. Mishra, G. Hota. Available online at: http://dspace.nitrkl.ac.in/dspace/bitstream/2080/1441/1/Electrospinning.pdf (accessed 16 May 2013).
[68] M.S. Yazdan Parast, A. Morsali. *Inorg. Chem. Commun.*, **14**, 450 (2011).
[69] S.K. Pasha, V.S.V. Satyanarayana, A. Sivakumar, K. Chidambaram, L.J. Kennedy. *Chin. Chem. Lett.*, **22**, 891 (2011).
[70] A.V. Borhadea, B.K. Uphadeb, D.R. Tope. *J. Chem. Sci.*, **125,** 583 (2013).
[71] L. Hashemi, A. Aslani, A. Morsali. *J. Inorg. Organomet. Polym. Mater.*, **22**, 867 (2012).
[72] A. Aslani, A. Morsali. *Inorg. Chim. Acta*, **362**, 5012 (2009).
[73] L. Hashemi, A. Morsali. *J. Coord. Chem.*, **64**, 4088 (2011).
[74] B. Mirtamizdoust, B. Shaabani, A. Khandar, H. Pourradi, Y. Abbasityula, H. Goudarziafshar, D. Viterbo, G. Croce, P. Hojati-Talemi. *J. Inorg. Organomet. Polym. Mater.*, **22**, 1293 (2012).
[75] B. Mirtamizdoust, B. Shaabani, A. Khandar, H.-K. Fun, S. Huang, M. Shadman, P. Hojati-Talemi. *Z. Anorg. Allg. Chem.*, **638**, 844 (2012).
[76] Y. Hanifehpour, B. Mirtamizdoust, S.W. Joo. *J. Inorg. Organomet. Polym. Mater.*, **22**, 816 (2012).
[77] H. Sadeghzadeh, A. Morsali. *Ultrason. Sonochem.*, **18**, 80 (2011).
[78] G.H. Shahverdizadeh, F. Hakimi, B. Mirtamizdoust, A. Soudi, P. Hojati-Talemi. *J. Inorg. Organomet. Polym. Mater.*, **22**, 903 (2012).
[79] A. Morsali, A. Panjehpour. *Inorg. Chim. Acta*, **391**, 210 (2012).
[80] E. Coronado, C. Martí-Gastaldo, J.R. Galán-Mascarós, M. Cavallini. *J. Am. Chem. Soc.*, **132**, 5456 (2010).
[81] A.D. Garnovskii, B.I. Kharisov (Eds.). *Direct Synthesis of Coordination and Organometallic Compounds*, p. 243, Elsevier Science, Lausanne (1999).
[82] V.G. Makhankova, O.V. Khavryuchenko, V.V. Lisnyak, V.N. Kokozay, V.V. Dyakonenko, O.V. Shishkin, B.W. Skelton, J. Jezierska. *J. Solid State Chem.*, **183**, 2695 (2010).
[83] S. Kumar, J.A. Azurdia, R.M. Laine. *J. Ceram. Proc. Res.*, **11**, 517 (2010).
[84] K. Liu, M. Zhong, F. Chen, Y. Shi, J. Yang. *Zhongguo Xitu Xuebao/J. Chin. Rare Earth Soc.*, **29**, 737 (2011).
[85] K. Liu, M. Zhong. *J. Rare Earths*, **28**, 680 (2010).
[86] S. Ghoshal, V.K. Jain. *J. Chem. Sci.*, **119**, 583 (2007).
[87] X. Shen, J. Sun, G. Wang, J. Park, K. Chen. *Mater. Res. Bull.*, **45**, 766 (2010).
[88] V. Resta, A.M. Laera, A. Camposeo, E. Piscopiello, L. Persano, D. Pisignano, L. Tapfer. *J. Phys. Chem. C*, **116**, 25119 (2012).
[89] A. Hosseinian, A.R. Mahjoub. *J. Mol. Struct.*, **985**, 270 (2011).
[90] A. Hosseinian, A.R. Mahjoub, M. Movahedi. *Int. J. Nano Dim.*, **1**, 65 (2010).
[91] P. Bera, C.H. Kim, S.I. Seok. *Solid State Sci.*, **12**, 532 (2010).
[92] R. Amutha, S. Akilandeswari, A.N. Kannappan, M. Muruganandham, M. Sillanpää. *Adv. Sci. Lett.*, **3**, 398 (2010).
[93] S.K. Maji, A.K. Dutta, S. Dutta, D.N. Srivastava, P. Paul, A. Mondal, B. Adhikary. *Appl. Catal., B*, **126**, 265 (2012).
[94] K.N. Sharma, H. Joshi, V.V. Singh, P. Singh, A.K. Singh. *Dalton Trans.*, 3908 (2013).
[95] N. Banerjee, S.B. Krupanidhi. *Mater. Chem. Phys.*, **137**, 466 (2012).
[96] M. Annie Freeda, N. Rode Madhav, C.K. Mahadevan, S. Ramalingom. *Nanotechnol. Nanosci.*, **1**, 4 (2010).
[97] M. Salavati-Niasari, B. Shoshtari-Yeganeh, F. Mohandes. *Mater. Res. Bull.*, **48**, 1745 (2013).
[98] G. Pandey, H.K. Sharma. *Synth. React. Inorg. Met.-Org. Nano-Met. Chem.*, **40**, 312 (2010).
[99] S.N. Malik, S. Mahboob, N. Haider, M.A. Malik, P. O'Brien. *Nanoscale*, **3**, 5132 (2011).
[100] M. Sacilotti, P. Cheyssac, G. Patriarche, J. Decobert, Th Chiaramonte, L.P. Cardoso, M.F. Pillis, M.J. Brasil, F. Iikawa, M. Nakaema, Y. Lacroute, J.C. Vial, F. Donatini. *Surf. Coat. Technol.*, **201**, 9104 (2007).
[101] A.P. Herrera, L. Polo-Corrales, E. Chavez, J. Cabarcas-Bolivar, O.N. Uwakweh, C. Rinaldi. *J. Magn. Magn. Mater.*, **328**, 41 (2013).
[102] I.V. Vasylenko, K.S. Gavrylenko, V.G. Il'yin, V. Golub, G. Goloverda, V. Kolesnichenko, A.W. Addison, V.V. Pavlishchuk. *Mater. Chem. Phys.*, **121**, 47 (2010).
[103] C.-G. Zhu, F.-W. Wang, M. Xu, W.-Y. Fang. *Chin. J. Inorg. Chem.*, **25**, 1177 (2009).
[104] A. Vecoven, A.W. Apblett. *Ceram. Trans.*, **227**, 263 (2011).
[105] U.B. Gawas, S.C. Mojumdar, V.M.S. Verenkar. *J. Therm. Anal. Calorim.*, **100**, 867 (2010).
[106] U.B. Gawas, V.M.S. Verenkar, S.C. Mojumdar. *J. Therm. Anal. Calorim.*, **108**, 865 (2012).
[107] U.B. Gawas, V.M.S. Verenkar, S.C. Mojumdar. *J. Therm. Anal. Calorim.*, **104**, 879 (2011).
[108] F. Wang, M. Xu, Y. Wei, W. Fang. *Chem. Bull./Huaxue Tongbao*, **74**, 750 (2011).
[109] D. Sarma, P. Mahata, N. Srinatarajan. *Curr. Sci.*, **14**, 450 (2012).
[110] M. Adil Mansoor, A. Ismail, R. Yahya, Z. Arifin, E.R.T. Tiekink, S.W. Ng, A. Reza Esmaeili, *Inorg. Chem.*, **52**, 5624 (2013).
[111] M. Kim, R.M. Laine. *J. Am. Chem. Soc.*, **131**, 9220 (2009).
[112] B.I. Kharisov, O.V. Kharissova, U. Ortiz-Mendez, *Handbook of Less-common Nanostructures*, p. 886, Taylor & Francis CRC Press, Boca Raton, Florida (2012).